

AD-A172 133

FEASIBILITY TEST PROGRAM FOR A HYDROFLEX (TRADE NAME)

1/1

BEARING(U) MECHANICAL TECHNOLOGY INC LATHAM N Y

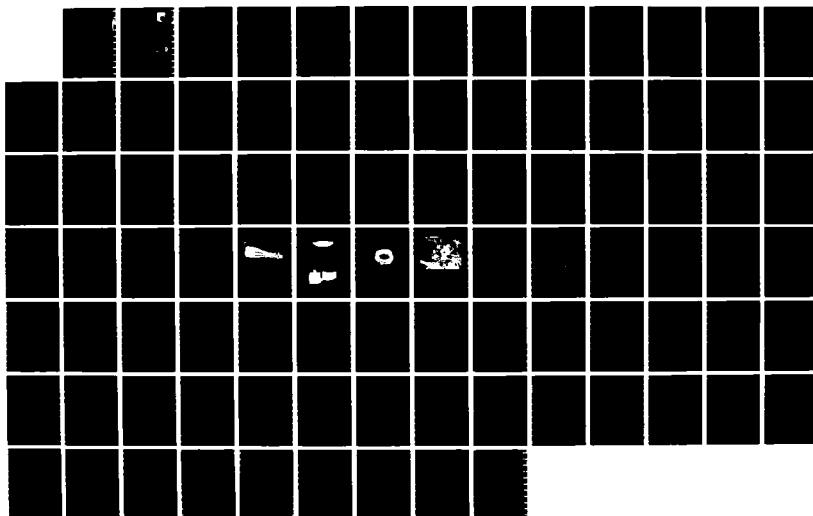
M H EUSEPI ET AL. MAY 86 NTI-86TR3 AFML-TR-86-2003

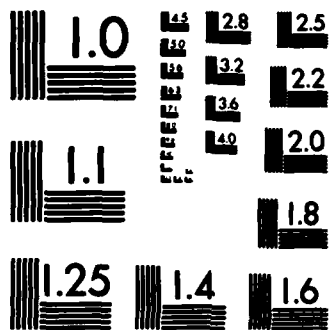
UNCLASSIFIED

F33615-84-C-2429

F/G 21/5

NL





1077

AFWAL-TR-86-2003

**AD-A172 133**

## **FEASIBILITY TEST PROGRAM FOR A HYDROFLEX™ BEARING**

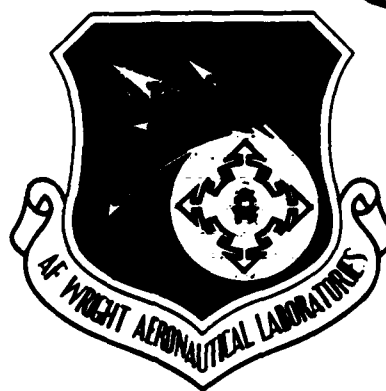
MARTIN W. EUSEPI  
DONALD F. WILCOCK

Mechanical Technology Incorporated  
968 Albany-Shaker Road  
Latham, New York 12110

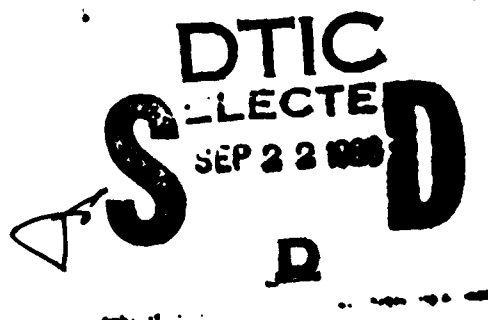
May 1986

Final Technical Report for Period July 1984 - June 1985

Approved for Public Release; Distribution Is Unlimited



12



**DTIC FILE COPY**

AERO PROPULSION LABORATORY  
AIR FORCE WRIGHT AERONAUTICAL LABORATORIES  
AIR FORCE SYSTEMS COMMAND  
WRIGHT-PATTERSON AIR FORCE BASE, OHIO 45433-6563

86 9 22 062

## NOTICE

When Government drawings, specifications, or other data are used for any purpose other than in connection with a definitely related Government procurement operation, the United States Government thereby incurs no responsibility nor any obligation whatsoever; and the fact that the government may have formulated, furnished, or in any way supplied the said drawings, specifications, or other data, is not to be regarded by implication or otherwise as in any manner licensing the holder or any other person or corporation, or conveying any rights or permission to manufacture, use, or sell any patented invention that may in any way be related thereto.

This report has been reviewed by the Office of Public Affairs (ASD/PA) and is releasable to the National Technical Information Service (NTIS). At NTIS, it will be available to the general public, including foreign nations.

This technical report has been reviewed and is approved for publication.

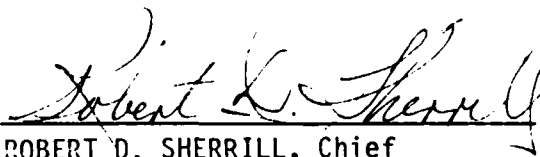


RONALD D. DAYTON  
Lubrication Systems Tech Area Mgr  
Lubrication Branch  
Fuels and Lubrication Division  
Aero Propulsion Laboratory



HOWARD F. JONES  
Chief, Lubrication Branch  
Fuels and Lubrication Division  
Aero Propulsion Laboratory

FOR THE COMMANDER:



ROBERT D. SHERRILL, Chief  
Fuels and Lubrication Division  
Aero Propulsion Laboratory

"If your address has changed, if you wish to be removed from our mailing list, or if the addressee is no longer employed by your organization please notify AFWAL/POSL, W-PAFB, OH 45433 to help us maintain a current mailing list."

Copies of this report should not be returned unless return is required by security considerations, contractual obligations, or notice on a specific document.

Unclassified

SECURITY CLASSIFICATION OF THIS PAGE

ADAM72133

## REPORT DOCUMENTATION PAGE

1a. REPORT SECURITY CLASSIFICATION Unclassified			1b. RESTRICTIVE MARKINGS		
2a. SECURITY CLASSIFICATION AUTHORITY			3. DISTRIBUTION/AVAILABILITY OF REPORT Approved for public release; Distribution is unlimited.		
2b. DECLASSIFICATION/DOWNGRADING SCHEDULE					
4. PERFORMING ORGANIZATION REPORT NUMBER(S) MTI 86TR3			5. MONITORING ORGANIZATION REPORT NUMBER(S) AFWAL-TR-86-2003		
6a. NAME OF PERFORMING ORGANIZATION Mechanical Technology Inc.		6b. OFFICE SYMBOL (If applicable)		7a. NAME OF MONITORING ORGANIZATION Aero Propulsion Laboratory (AFWAL/POSL) AF Wright Aeronautical Laboratories	
6c. ADDRESS (City, State, and ZIP Code) 968 Albany-Shaker Road Latham, New York 12110				7b. ADDRESS (City, State, and ZIP Code) Wright-Patterson Air Force Base OH 45433	
8a. NAME OF FUNDING/SPONSORING ORGANIZATION Aero Propulsion Laboratory		8b. OFFICE SYMBOL (If applicable)		9. PROCUREMENT INSTRUMENT IDENTIFICATION NUMBER F33615-84-C-2429	
8c. ADDRESS (City, State, and ZIP Code) Fuels & Lubrications Div. (AFWAL/POSL) AF Wright Aeronautical Laboratories WPAFB, OH 45433-6563		10. SOURCE OF FUNDING NUMBERS			
		PROGRAM ELEMENT NO. PE 61101F		PROJECT NO. 0100	TASK NO. P4
				WORK UNIT ACCESSION NO. 09	
11. TITLE (Include Security Classification) FEASIBILITY TEST PROGRAM FOR A HYDROFLEX™ BEARING					
12. PERSONAL AUTHOR(S) Martin W. Eusepi and Donald F. Wilcock					
13a. TYPE OF REPORT Final		13b. TIME COVERED FROM July 84 to June 85		14. DATE OF REPORT (Year, Month, Day) May 1986	
15. PAGE COUNT 89					
16. SUPPLEMENTARY NOTATION					
17. COSATI CODES			18. SUBJECT TERMS (Continue on reverse if necessary and identify by block number)		
FIELD	GROUP	SUB-GROUP	Bearing Hydrodynamic Gas Bearing		
			Gas Bearing Partial-Arc Bearing Bearing Friction Damper		
			Pad Bearing Resilient Bearing Bearing Damper		
19. ABSTRACT (Continue on reverse if necessary and identify by block number)					
<p>The Hydroflex bearing concept consists of a conventionally shaped, partial-arc gas bearing permanently attached to a leaf-spring-shaped flexure via a small-cross-section short post. When assembled into a complete bearing, small friction pads are installed so they press against the lateral face of the flexure. The Coulomb friction generated by these small flat pads provides damping for the reduction of rotor response amplitudes in the area of a critical speed.</p> <p>The program was promulgated to establish the feasibility of the Hydroflex bearing concept. To reach the objective of this program, the following tasks were accomplished:</p> <ul style="list-style-type: none"> <li>o Design of Hydroflex bearing;</li> <li>o Design of test rig and fabrication of test components;</li> <li>o Experimental evaluation of Hydroflex bearing concept.</li> </ul> <p><i>Hydroflex gas bearing concept, showing the Coulomb friction damping.</i></p>					
20. DISTRIBUTION/AVAILABILITY OF ABSTRACT <input checked="" type="checkbox"/> UNCLASSIFIED/UNLIMITED <input type="checkbox"/> SAME AS RPT. <input type="checkbox"/> OTC USERS			21. ABSTRACT SECURITY CLASSIFICATION Unclassified/Unlimited		
22a. NAME OF RESPONSIBLE INDIVIDUAL			22b. TELEPHONE (Include Area Code)		22c. OFFICE SYMBOL

## SUMMARY

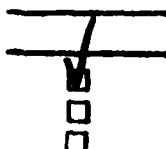
The Hydroflex™ gas bearing design provides substantial, controlled damping to a design that retains the resiliency of a foil bearing, while providing the dimensional control of a rigid bearing. It consists of a conventionally shaped, partial-arc air bearing that is permanently attached to a leaf-spring-shaped flexure via a small-cross-section short post. When assembled into a complete bearing, small friction pads mounted on spring arms are installed so that they press against the lateral face of the flexure. The Coulomb friction generated by these small flat pads provides damping for the reduction of rotor response amplitudes near a critical speed.

The feasibility demonstration was implemented with a bearing designed for a 3.5-in. diameter journal that was loaded using shaft weight only. A tester configuration providing an additional support bearing and an air turbine drive was also designed and fabricated in conjunction with the design of the Hydroflex bearing. The final bearing design resulted in four equally spaced pads; 3.50 in. diameter; 2.00 in. length; a clearance ratio of  $2.0 \times 10^{-3}$  in./in.; a preload ratio of 0.6; a pivot location 55% from the leading edge; and a flexure radial stiffness of 6690 lb/in.

The results of a critical speed analysis showed that there are two critical speeds below the target speed of 30,000 r/min. The first, a conical mode with its apex at the fluid film support bearing, is at a low speed. The second, at almost 17,000 r/min, also has a conical mode, but its apex is at the Hydroflex bearing.

The Hydroflex bearing was tested according to a matrix that called for data to be taken at rotor speeds from 3,300 to 30,000 r/min, with and without external damping, and with rotor unbalances at the Hydroflex bearing extending from a residual of 0.002 to 0.032 in.-oz. For each of the tests conducted with external damping, the damper springs were adjusted to provide a 3-lb static radial friction force at each bearing pad.

In all cases, the addition of external Coulomb damping reduced the low-speed critical speed response. At low external unbalance levels (below 0.016 in.-oz), both the vertical and horizontal response amplitude seemed to be



Codes

Dist      new and/or  
Special

A-1

critically damped. Above 0.016 in.-oz unbalance, calculations were based on the half-power point width of the response curve at the critical speed. The results of these calculations, taken from actual Hydroflex bearing test data, are:

Unbalance (in.-oz)	External Damping (lb)	Damping Ratio	Damping Coefficient (lb-s/in.)
0.016	0	0.095	5.4
0.016	3	0.49	28.1
0.032	0	0.12	6.88
0.032	3	0.21	12.00

The response of the test rotor at the second higher critical speed was quite flat with no evidence of response amplification. Additionally, there was no response amplification resulting from the 0.2 g excitation imposed at or near one-half running speed at any test speed.

To close out the experimental program, the Hydroflex bearing was run to 30,000 r/min with 0.032 in.-oz unbalance at the Hydroflex bearing location. No instabilities were noted in the run to 30,000 r/min and, with the successful completion of this final test, the experimental program was concluded.

## PREFACE

This final report describes the work performed by Mechanical Technology Incorporated, 968 Albany-Shaker Rd., Latham, New York 12110, under U.S. Air Force Contract F33615-84-C-2429. The report covers the period from July 1984 through June 1985.

This feasibility study of the Hydroflex air bearing concept was sponsored by the Aero Propulsion Laboratory of the Air Force Wright Aeronautical Laboratories (AFWAL), Wright-Patterson Air Force Base, Ohio 45433-6563 as In-House Laboratory Independent Research. Lt. G. Gainer and Capt. D. Koretsky were the USAF AFWAL/POSL project engineers. The work at Mechanical Technology Incorporated was performed by M. Eusepi, the principal investigator, and Dr. D. Wilcock, consultant.



## TABLE OF CONTENTS

<u>SECTION</u>	<u>PAGE</u>
1.0 INTRODUCTION . . . . .	1
2.0 HYDROFLEX BEARING DESIGN ANALYSIS . . . . .	3
2.1 Bearing Parameters . . . . .	3
2.1.1 Single-Pad Behavior . . . . .	4
2.1.2 Opposed-Pad Behavior . . . . .	8
2.1.3 Pivot Offset . . . . .	14
2.1.4 The Assembled Four-Pad Bearing . . . . .	14
2.1.5 Unbalance Behavior . . . . .	20
2.2 Flexure Design . . . . .	22
3.0 TEST VEHICLE DESIGN . . . . .	26
4.0 EXPERIMENTAL EVALUATION OF THE HYDROFLEX BEARING . . . . .	48
4.1 Static Spring Rate Measurements . . . . .	48
4.2 Dynamic Evaluation of Damping Rate and Rotor Unbalance Response . . . . .	48
4.3 Effects of External Excitation . . . . .	70
5.0 DISCUSSION OF TEST RESULTS . . . . .	74
6.0 CONCLUSIONS AND RECOMMENDATIONS . . . . .	78

## LIST OF ILLUSTRATIONS

<u>NUMBER</u>		<u>PAGE</u>
2-1	Single-Pad Air Bearing on a Flexure Pivot . . . . .	6
2-2	Flexure Stiffness vs Leading Edge Angle for 80° Pad and L/D = 0.57 . . . . .	7
2-3	Flexural Stiffness vs Leading Edge Angle for 80° Pad and L/D = 0.57 . . . . .	10
2-4	Pad Load and Minimum Film Thickness vs Eccentricity Ratio . . . .	11
2-5	Stiffness of Opposed Pads on Rigid Mounts . . . . .	12
2-6	Stiffness of Opposed Pads Supported on Radial Spring Flexures . .	13
2-7	Pad Load vs Eccentricity Ratio for 40° and 45° Pivot Position for a 2000 in.-lb/rad Flexure . . . . .	15
2-8	Hydroflex Bearing . . . . .	18
2-9	Hydroflex™ Bearing Flexure Design . . . . .	23
2-10	Analytical Model of Flexure Pad Support . . . . .	24
3-1	Hydroflex™ Bearing Test Vehicle . . . . .	27
3-2	Hydroflex™ Bearing Pad Thermocouple Orientation . . . . .	28
3-3	Instrumentation Schematic . . . . .	29
3-4	Rotordynamic Model . . . . .	30
3-5	Critical Speed Map - Hydroflex™ Bearing Tester - Ball Bearing Assembly . . . . .	32
3-6	Test Rotor Assembly . . . . .	34
3-7	Hydroflex™ Bearing Pad . . . . .	35
3-8	Hydroflex™ Bearing Assembly . . . . .	36
3-9	Hydroflex™ Test Apparatus . . . . .	37
3-10	Experimental Response Curve - Ball Bearing Assembly . . . . .	39
3-11	Critical Speed Map - Hydroflex™ Bearing Tester - Fluid Film Bearing Assembly . . . . .	43
3-12	Analytical Rotor Response - Fluid Film Bearing Assembly, Stations 1, 2, & 8 . . . . .	45
3-13	Analytical Rotor Response - Fluid Film Bearing Assembly, Stations 5, 12, & 15 . . . . .	46
4-1	Test Setup for Hydroflex™ Pad Stiffness Measurement . . . . .	49
4-2	Test Setup for Hydroflex™ Bearing Component Stiffness Measurement . . . . .	50

# LIST OF ILLUSTRATIONS (Continued)

<u>NUMBER</u>		<u>PAGE</u>
4-3	Hydroflex™ Bearing Response; External Damping - with and without Energy Absorbing Foam Backing . . . . .	54
4-4	Unbalance Response; No External Unbalance; with and without External Damping . . . . .	55
4-5	Unbalance Response; $4 \times 10^{-3}$ in.-oz External Unbalance; with and without External Damping . . . . .	56
4-6	Unbalance Response; $8 \times 10^{-3}$ in.-oz External Unbalance; with and without External Damping . . . . .	57
4-7	Unbalance Response; $16 \times 10^{-3}$ in.-oz External Unbalance; with and without External Damping . . . . .	58
4-8	Unbalance Response; $32 \times 10^{-3}$ in.-oz External Unbalance; with and without External Damping . . . . .	59
4-9	Unbalance Response; with External Damping; with and without $2 \times 10^{-3}$ in.-oz External Unbalance . . . . .	60
4-10	Unbalance Response; with External Damping; with and without $4 \times 10^{-3}$ in.-oz External Unbalance . . . . .	61
4-11	Unbalance Response; with External Damping; with and without $8 \times 10^{-3}$ in.-oz External Unbalance . . . . .	62
4-12	Unbalance Response; with External Damping; with and without $16 \times 10^{-3}$ in.-oz External Unbalance . . . . .	63
4-13	Unbalance Response; with External Damping; with and without $32 \times 10^{-3}$ in.-oz External Unbalance. . . . .	64
4-14	Unbalance Response; No External Damping; with and without $4 \times 10^{-3}$ in.-oz External Damping . . . . .	65
4-15	Unbalance Response; No External Damping; with and without $8 \times 10^{-3}$ in.-oz External Damping . . . . .	66
4-16	Unbalance Response; No External Damping; with and without $16 \times 10^{-3}$ in.-oz External Damping . . . . .	67
4-17	Unbalance Response; No External Damping; with and without $16 \times 10^{-3}$ in.-oz External Damping . . . . .	68
4-18	External Excitation Test Setup . . . . .	71

# LIST OF TABLES

NUMBER		PAGE
2-1	SINGLE-PAD RESULTS FROM PN399; $\Lambda = 1.0$ . . . . .	5
2-2	SINGLE-PAD RESULTS FROM PN399; $\Lambda = 0.2$ . . . . .	9
2-3	PREDICTED PERFORMANCE OF FOUR-PAD HYDROFLEX™ BEARING . . . . .	17
2-4	PREDICTED HYDROFLEX™ PERFORMANCE versus LOAD . . . . .	21
2-5	PREDICTED ECCENTRICITY versus LOAD FOR HYDROFLEX™ BEARING . . . .	21
3-1	HYDROFLEX™ STIFFNESS - CRITICAL SPEED RELATIONSHIP; BALL BEARING DESIGN . . . . .	33
3-2	CALCULATED DATA FOR OIL-LUBRICATED SUPPORT BEARING . . . . .	42
3-3	HYDROFLEX™ STIFFNESS - CRITICAL SPEED RELATIONSHIP; FLUID FILM BEARING DESIGN . . . . .	44
4-1	MEASURED STIFFNESS - HYDROFLEX™ BEARING . . . . .	51
4-2	HYDROFLEX™ BEARING DYNAMIC TEST MATRIX . . . . .	51
4-3	TYPICAL PAD TEMPERATURE RECORDED DURING THE TEST PROGRAM . . . .	69
4-4	EXTERNAL EXCITATION TEST RESULTS . . . . .	72
5-1	EXPERIMENTAL DAMPING COEFFICIENTS FOR THE HYDROFLEX™ BEARING . .	76

## NOMENCLATURE

B	Damping coefficient, lb-sec/in.
C	Radial clearance, in.
D	Diameter, in.
f	Excitation frequency, r/min
g	Acceleration ratio
h	Film thickness, in.
K	Stiffness, lb/in.
$K_{\xi}$	Angular stiffness, in.-lb/rad
L	Length, in.
M	Rotor mass, lb-sec <sup>2</sup> /in.
$M_R$	Moment, in.-lb
N	Rotation frequency, r/min
$P_a$	Ambient pressure, lb/in. <sup>2</sup>
Q	Resonance factor
R	Bearing radius, in.
r	Damping ratio
$U_x$	Unbalanced quantity, in.-oz
W	Load, lb
$\delta$	Log decrement
$\epsilon$	Eccentricity
$\theta$	Angle
$\Lambda$	Air bearing performance parameter, nondimensional
$\mu$	Viscosity, lb-sec/in. <sup>2</sup>
$\xi$	Angle, degree
$\phi$	Angle
$\omega$	Angular velocity, rad/sec

### Subscripts

c	Critical
f	Final
FL	Flexure
i	Initial
n	At maximum response
p	Pivot
xx	In direction of load

## 1.0 INTRODUCTION

The introduction of gas-lubricated bearings into high-speed turbomachinery has been prompted by the advantages of reduced system weight by virtue of the elimination of liquid lubrication hardware, the possibility of elevated temperature, operation, reduced power loss and long shelf life. The use of foil bearings as opposed to rigid designs, in addition to the usual gas bearing advantages, now provides the turbomachine designer with bearings that provide a high degree of tolerance to centrifugal growth and to differential thermal expansion, plus the resilience to take shock loading without bearing damage, all without a penalty in load-carrying capability.

Despite these advantages, some serious difficulties remain, particularly the following three.

1. There is a very limited amount of damping in either a rigid or a foil-type gas bearing. Damping is difficult to supply for the most useful applications: those operating at high temperature, where external squeeze-film or elastomer dampers cannot be used. The limited internal damping leads to a sensitivity both to unbalance and to rotor-bearing instability. As a result, precision balancing and great care in coupling the rotor design with the detailed bearing design is required in order to attain stable operation.
2. Fabrication is difficult in larger size foil bearings due to problems of warping of the curved foils and to the maintenance of accurate shape control.
3. Only very approximate theoretical predictions can be made for foil bearings because of problems associated with predicting compliance accurately over the foil for coupling with Reynolds equations.

In view of these difficulties, MTI conceived the Hydroflex gas bearing design as a means of achieving a substantial and controlled degree of damping, while retaining both the excellent resilient characteristics of the foil bearing (i.e., tolerance of dimensional change and shock) and simultaneously

retaining the dimensional control of the rigid bearing. Furthermore, the design permits the use of well-established rigid air bearing and rotordynamics design analyses.

The Hydroflex bearing concept consists of a conventionally shaped, partial-arc gas bearing permanently attached to a leaf-spring-shaped flexure via a small-cross-section short post. When assembled into a complete bearing, small friction pads are installed so they press against the lateral face of the flexure. The Coulomb friction generated by these small flat pads provides damping for the reduction of rotor response amplitudes in the area of a critical speed.

The program described herein was promulgated to establish the feasibility of the Hydroflex bearing concept. To reach the objective of this program, the following tasks were accomplished:

- Design of Hydroflex bearing.
- Design of test rig and fabrication of test components.
- Experimental evaluation of Hydroflex bearing concept.

## 2.0 HYDROFLEX BEARING DESIGN ANALYSIS

The design analyses required by the Hydroflex<sup>™</sup> feasibility demonstration program for the bearing and its supporting flexures are presented in this section. These include the response of a single pad when restrained by a moment at the 'pivot' position, the design of the compound flexure to provide both angular and radial compliance, the predicted behavior of the full bearing, and the design of a stable oil-lubricated support bearing at the drive end of the test rotor. No new computer codes were required for this work.

### 2.1 Bearing Parameters

The shaft diameter selected for this program was 3.5 in. in order to demonstrate the capability of the Hydroflex design approach to function on large-diameter shafts. An initial load estimate of 18 lb per bearing was made. In order to maintain the starting load in the usual range of 1 to 2 psi based on the projected area, the bearing length was set at 2.00 in.

Four pads, each subtending an arc of 80°, were selected for the complete Hydroflex bearing. A radial clearance of 0.0035 in. was chosen, providing a C/R ratio of 0.002 based on the machined-in clearance. The pad pivot points are set on diagonals 45° from vertical.

The principal parameter controlling the performance parameters of an air bearing is  $\Lambda$ , given by Equation (2-1) below:

$$\Lambda = 6\mu\omega/P_a (R/C)^2 \quad (2-1)$$

Using the viscosity of air at 200°F,  $3.0 \times 10^{-9}$  lb-s/in.<sup>2</sup>, and an angular velocity of 3142 rad/s (30,000 r/min),  $\Lambda$  is found to be 0.96.



### 2.1.1 Single-Pad Behavior

Using MTI CADENSE® 40\*, a number of single-pad performance calculations were made at  $\Lambda = 1.0$ . These were made for a series of film thickness ratios over the pivot, and for several values of the pivot position. The results are shown in Table 2-1 in terms of both the non-dimensional and dimensional terms.

The key dimensions and forces are shown in Figure 2-1. This figure shows the pad with the supporting flexure pivot located at  $180^\circ$  and with the shaft-applied load vertically downward. The pad is tilted as shown in the counter-clockwise direction, the point of reaction to the shaft load being shifted leftward by an amount,  $\Delta L$ . This results in a moment, which is just sufficient to bend the flexure and thus tilt the pad. The computer code calculates the results for the case of a frictionless pivot located at  $180^\circ$ . For a symmetrical  $80^\circ$  pad this would put the pad leading edge angle at  $140^\circ$ . The effect of the flexure is simulated by making the leading edge angle somewhat smaller or somewhat larger. The bearing resultant force is then shifted from the flexure location by an amount,  $\Delta L$ .

The tilt angle can be calculated by using the film thickness at the pivot and the film thickness at the minimum film point on the line of centers. Equation (2-2) is used to calculate the tilt angle,  $\xi$ :

$$\xi = \epsilon (C/R) (1 - \cos \phi) / \sin \phi / \cos \phi \quad (2-2)$$

Knowing the tilt angle and the moment,  $W \times \Delta L$ , the flexure stiffness required to support this pad position is obtained.

The results of these calculations are also shown in Table 2-1. Since this type of bearing will be assembled with a built-in preload, the results at  $\epsilon = 0.5$  are of greatest interest; and these are plotted in terms of flexure stiffness versus leading edge angle in Figure 2-2. A husky pivot,  $0.15 \times 0.15$  in. in cross-section, has an angular stiffness of about 2,000 in.-lb/rad. This

\*CAD-40 = Performance of Gas-Lubricated Journal Bearings. CADENSE® is an acronym for Computer-Aided Design Engineering Services.

TABLE 2-1

SINGLE-PAD RESULTS FROM PN399;  $\Lambda = 1.0$   
(Pivot at  $180^\circ$ ,  $D = 3.5$ ,  $L = 2.0$ ,  $C = 0.002$ )

Initial Pad Angle $\theta_i$	Final Pad Angle $\theta_f$	Film Thickness Parameter $\epsilon \cos \phi$	Attitude Angle $\phi$	Dimensionless Quantities		Load $W$ (lb)	Load Offset $\Delta L$ (in.)	Pitch Moment $M_R$ (in.-lb)	Film Thickness $h_{min}$ (mils)	Tilt Angle ( $\text{rad} \times 10^3$ )	Angular Stiffness $K_\xi$ (in.-lb/rad)
				Film Thickness $\bar{h}_{min}$	Load $\bar{W}$						
145	225	0.5	19.2	0.4705	0.0278	2.86	0.153	0.436	0.94	0.189	2,310
		0.8	5.51	0.1911	0.1563	16.1	0.153	2.46	0.38	0.122	20,200
		0.9	4.56	0.0971	0.359	36.9	0.153	5.65	0.19	0.072	78,300
142	222	0.5	20.5	0.466	0.0331	3.41	0.061	0.21	0.93	0.206	1,020
138	218	0.5	24.1	0.452	0.0426	4.38	-0.061	-0.207	0.90	0.256	-1,040
135	215	0.5	28.6	0.430	0.0519	5.34	-0.153	-0.814	0.86	0.331	-2,460

NOTE: PN399, Static P Dynamic Performance of Hydrostatic Gas Bearings, is an MTI computer program



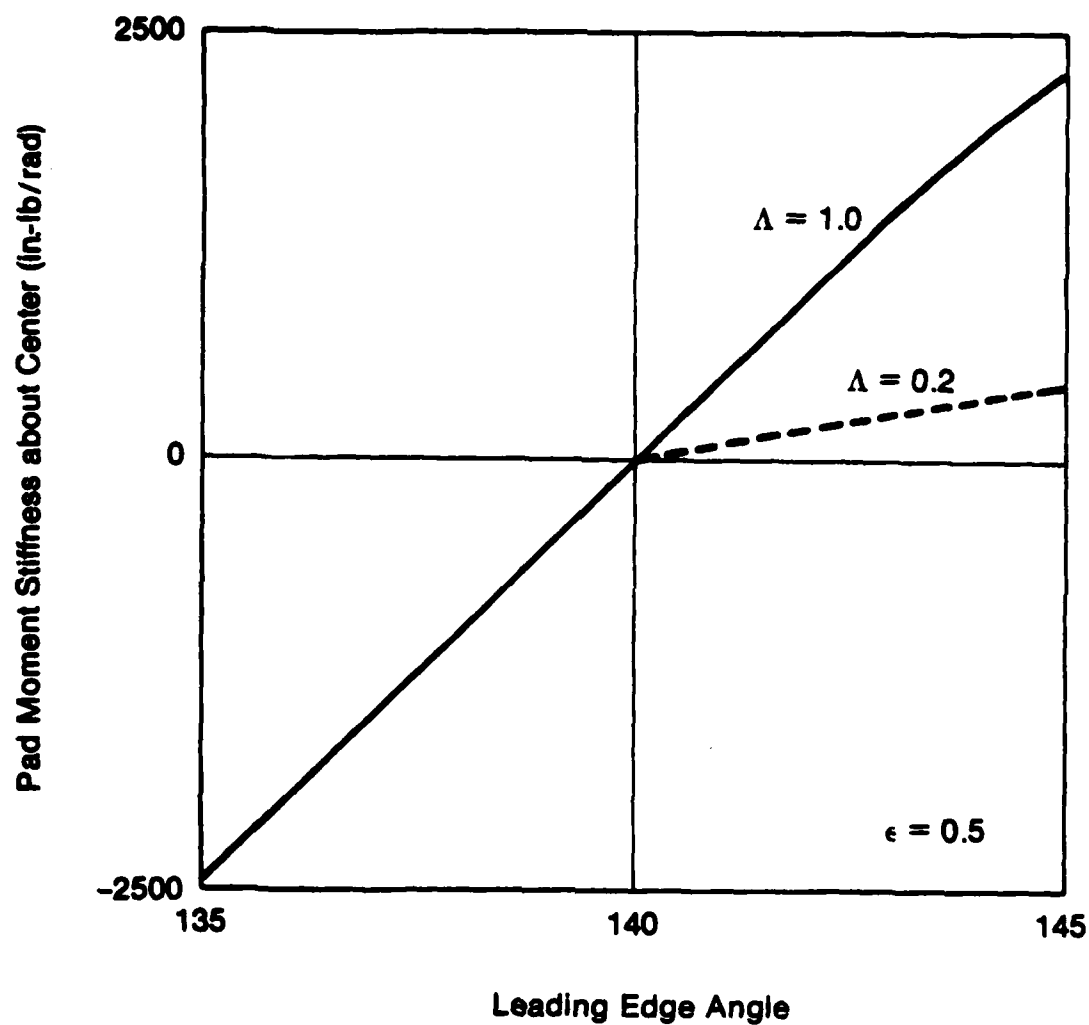


Fig. 2-2 Flexure Stiffness vs Leading Edge Angle for 80° Pad and  $L/D = 0.57$

corresponds to a shift of the load vector of slightly more than two degrees at an eccentricity ratio of 0.5. The shift will be much less at higher eccentricity ratios.

At the other end of the desired speed range, at a speed of 6,000 r/min,  $\Lambda$  is 0.2. The results of similar calculations at this speed are shown in Table 2-2, and plotted in Figure 2-2. It is apparent that the alignment stiffness required is lower than at the higher  $\Lambda$  value. With a 2,000 in.-lb/rad pivot, the pad deflection will be smaller and the preload smaller. The bearing is safe under this condition, as is shown in Figure 2-3 for the moment stiffness of the pad as a function of the leading edge angle. While the moment stiffness at  $\epsilon = 0.5$  is small, Figure 2-3 shows that at  $\epsilon = 0.8$ , the pivot stiffness of 2,000 lb/in. is met with an offset of less than three degrees. At  $\epsilon = 0.9$ , the required offset is only about half a degree.

Figure 2-4 shows the rapid increase in load carried as the eccentricity ratio is increased. This figure also illustrates the corresponding drop in minimum film thickness which occurs at the trailing edge of the pad.

### 2.1.2 Opposed-Pad Behavior

The film stiffness of the bearing pad is crucial to the concept of the Hydroflex bearing. In this concept, the bearing stiffness is desired to be high compared to the support stiffness. The stiffnesses are shown in Figure 2-5 as a function of eccentricity ratio for a pair of opposed pads at  $\Lambda = 0.2$ . Curves for preload ratios of zero, 0.5 and 0.65 are shown. Above  $\epsilon = 0.8$  and for stiffnesses above 30,000 lb/in., the three preloads fall on a single curve. If a preload of 0.5 is introduced, the curve starts at  $\epsilon = 0.5$  at a stiffness of 3,300, as shown. For a preload of 0.65, the curve starts at  $\epsilon = 0.65$  and a stiffness of 19,000. For this reason, the test bearing was assembled with a preload setting between 0.60 and 0.65.

The behavior of two opposed pads supported on flexure mounts is shown in Figure 2-6 for  $\Lambda = 0.2$  and a preload of 0.65. It is assumed that each pad is supported on a flexure with a radial spring stiffness of either 6,000 or 9,000 lb/in., so that the combined flexure stiffness for the two pads is either

TABLE 2-2

SINGLE-PAD RESULTS FROM PN399;  $\Lambda = 0.2$   
(Pivot at  $180^\circ$ ,  $D = 3.5$ ,  $L = 2.0$ ,  $C = 0.002$ )

Initial Pad Angle $\theta_i$	Final Pad Angle $\theta_f$	Film Thickness Parameter $\epsilon \cos \phi$	Attitude Angle $\phi$	Dimensionless Quantities		Load $W$ (lb)	Load Offset $\Delta L$ (in.)	Pitch Moment $M_R$ (in.-lb)	Film Thickness $h_{min}$ (mils)	Tilt Angle (rad $\times 10^3$ )	Angular Stiffness $K_\zeta$ (in.-lb/rad)
				Film Thickness $\bar{h}_{min}$	Load $\bar{W}$						
140	220	0.2	45.5	0.716	0.00226	0.23	0	0	2.51	0.340	0
		0.5	28.7	0.430	0.00978	1.01	0	0	1.51	0.332	0
		0.8	16.3	0.167	0.0680	7.00	0	0	0.585	0.249	0
		0.9	10.2	0.0856	0.193	19.9	0	0	0.300	0.166	0
142	222	0.5	26.9	0.439	0.00869	0.894	0.061	0.0545	1.54	0.301	181
144	224	0.5	25.7	0.445	0.00775	0.797	0.122	0.0972	1.56	0.281	346
145	225	0.5	25.3	0.447	0.00734	0.755	0.153	0.116	1.56	0.275	422
144.5	224.5	0.8	16.6	0.165	0.0619	6.37	0.137	0.873	0.578	0.244	3580
		0.9	10.5	0.0847	0.179	18.4	0.137	2.52	0.296	0.168	15,000
135	215	0.5	35.2	0.388	0.0132	1.36	-0.153	-0.208	1.36	0.388	-5360
		0.8	16.8	0.164	0.0765	7.87	-0.153	-1.204	0.574	0.247	-4880
		0.9	10.2	0.0855	0.210	21.6	-0.153	-3.305	0.299	0.163	-20,200

NOTE: PN399, Static P Dynamic Performance of Hydrostatic Gas Bearings, is an MTI computer program

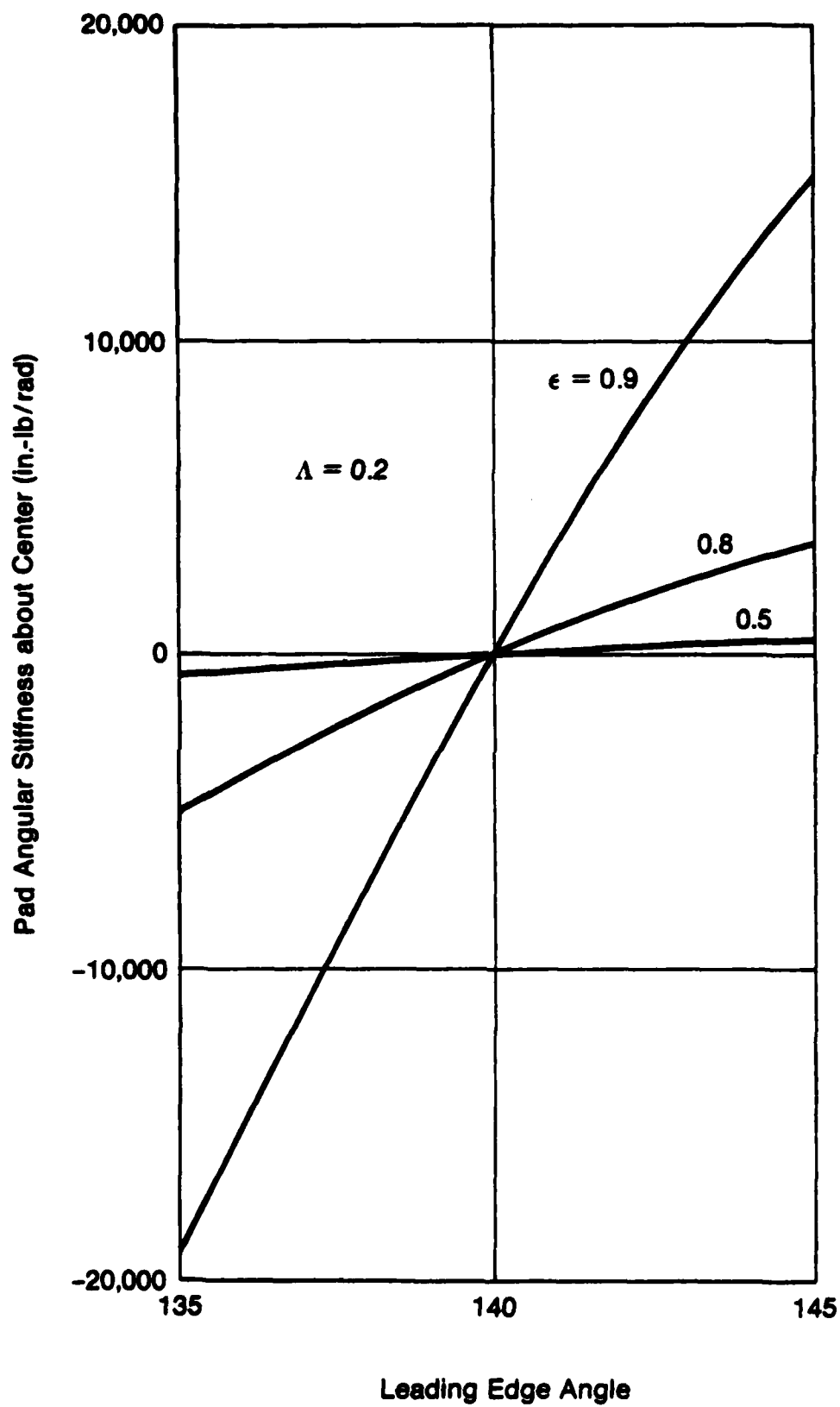


Fig. 2-3 Flexural Stiffness vs Leading Edge Angle  
for 80° Pad and  $L/D = 0.57$

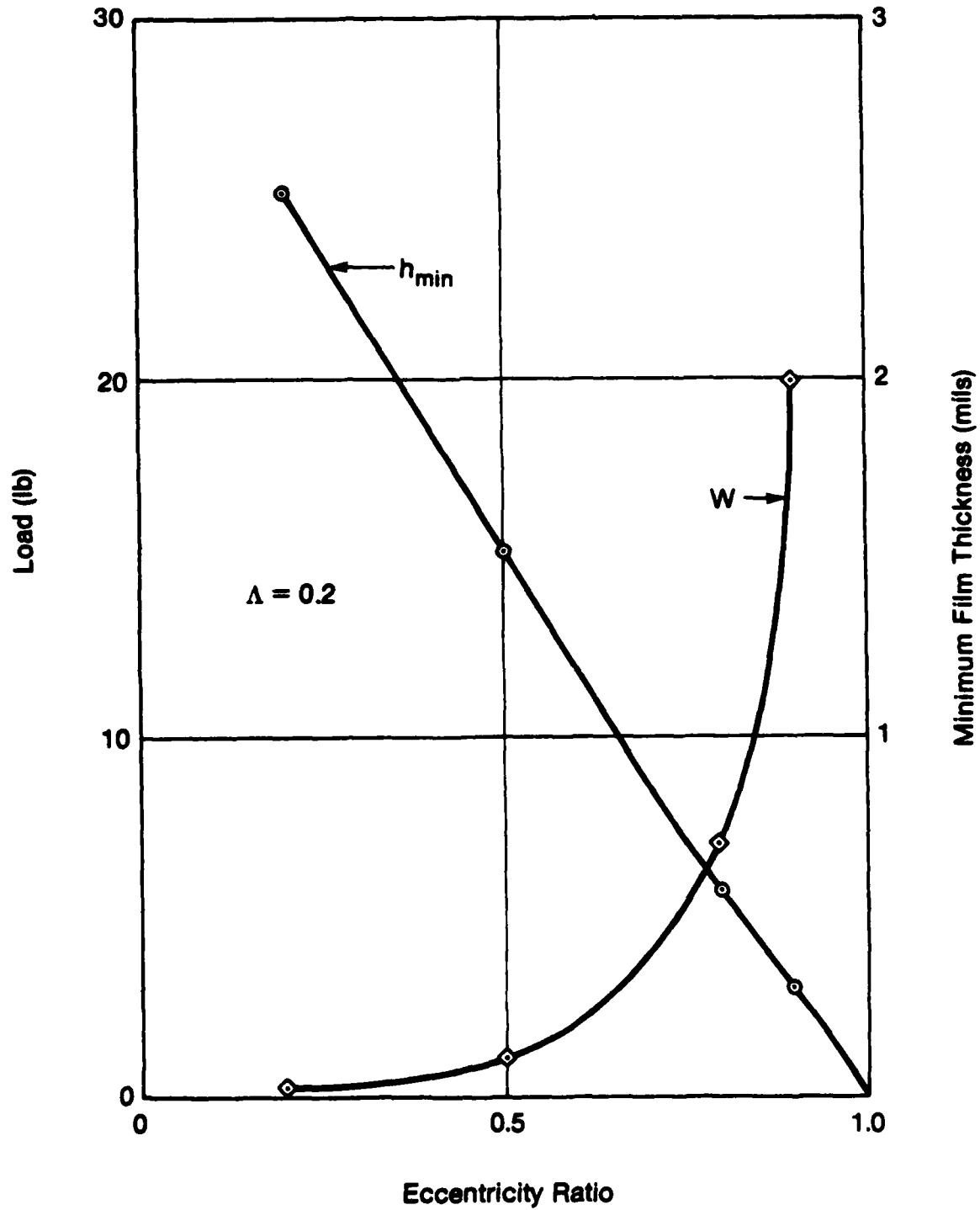


Fig. 2-4 Pad Load and Minimum Film Thickness vs Eccentricity Ratio



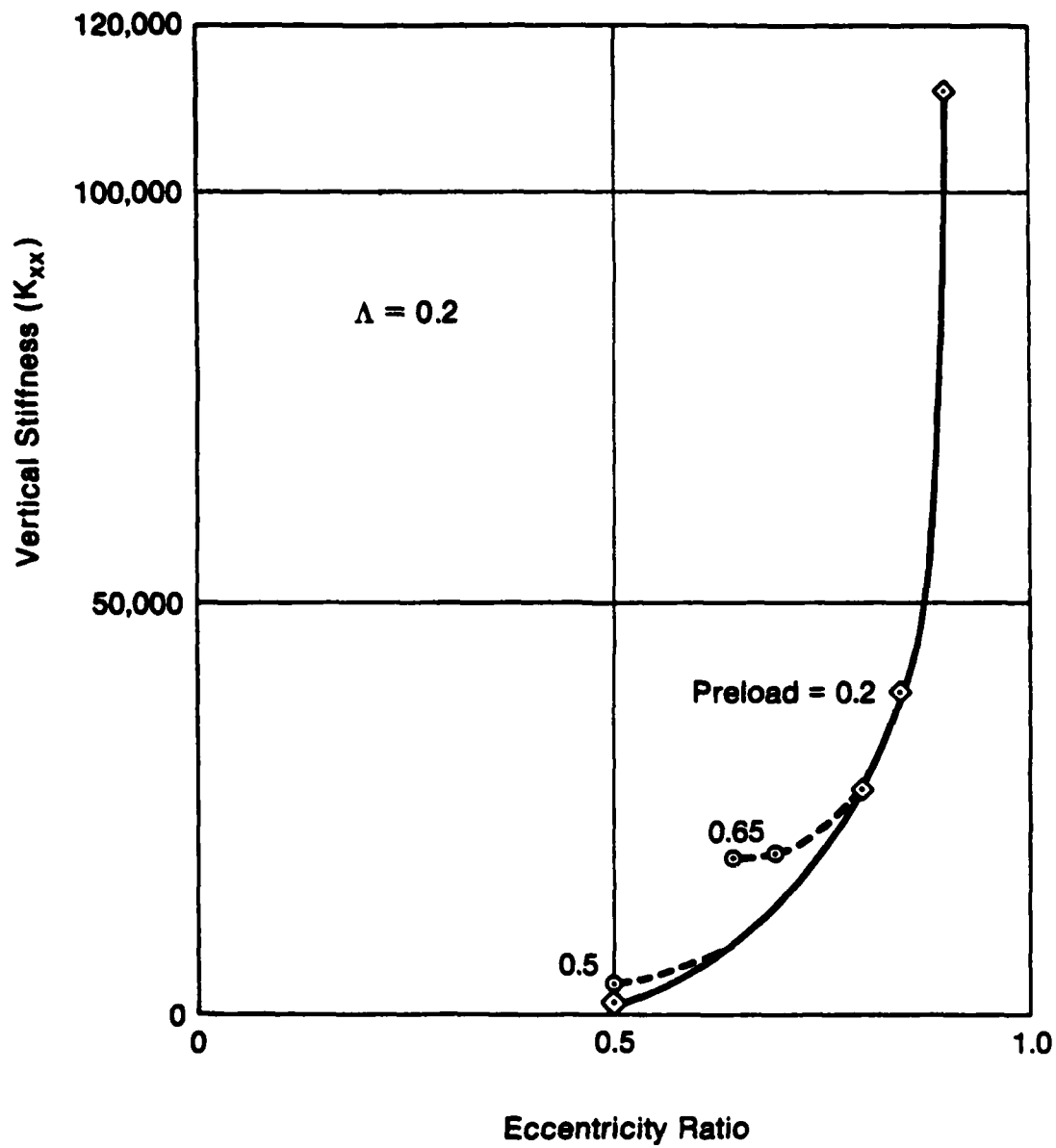


Fig. 2-5 Stiffness of Opposed Pads on Rigid Mounts

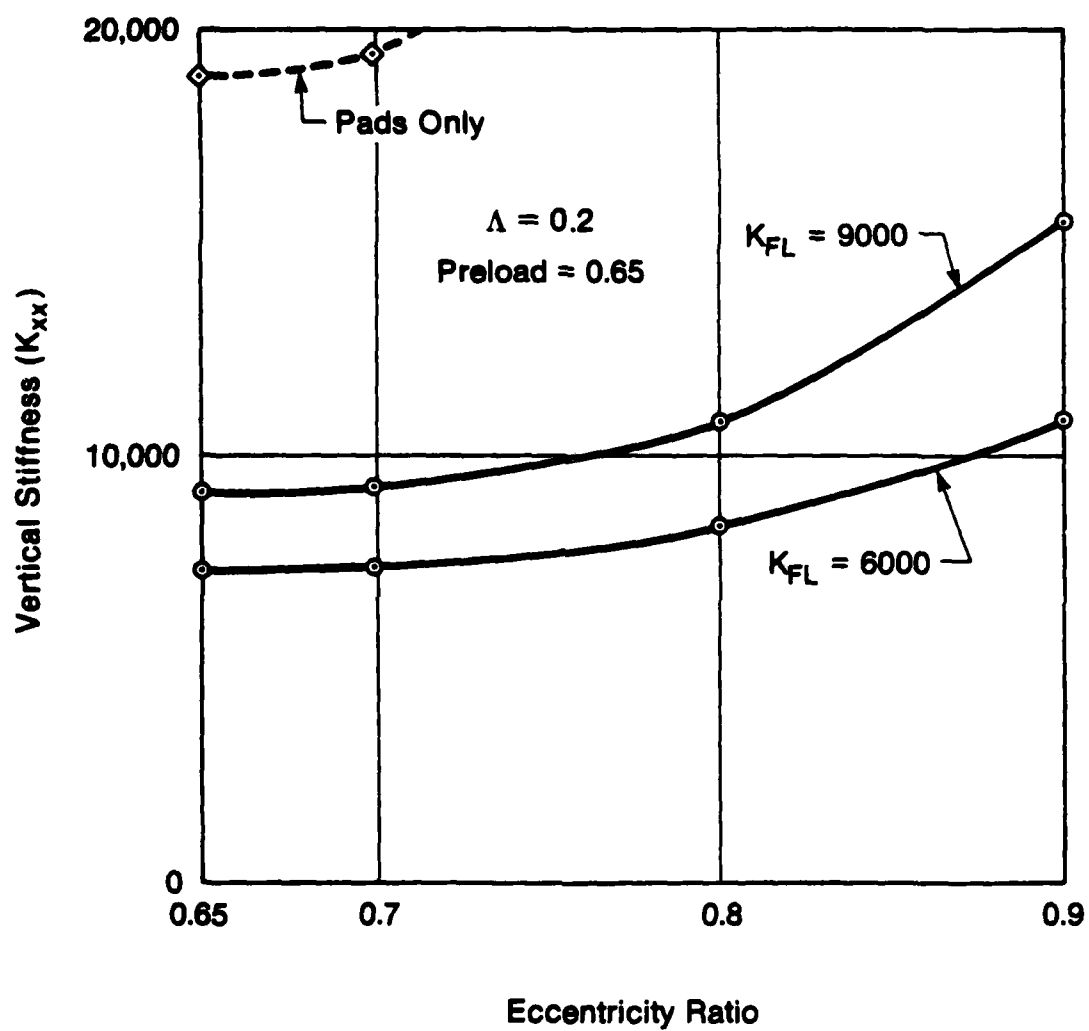


Fig. 2-6 Stiffness of Opposed Pads Supported on Radial Spring Flexures

12,000 or 18,000 lb/in. The combined bearing stiffness, for example, is shown as the solid curve starting at about 9,000 lb/in. and increasing to about 15,500 lb/in. at  $\epsilon = 0.9$ . A portion of the curve for the air film stiffness of the two pads is shown in the upper left corner.

### 2.1.3 Pivot Offset

Gas journal bearing pads, if only required to operate in one direction, are generally pivoted at the 55% point. In the case of the Hydroflex bearing with a flexure pivot having moment stiffness, the bearing reaction must come in advance of the pivot location by an amount varying with the eccentricity ratio. For these reasons, it was decided to place the flexure pivot at the 55% position or at the  $44^\circ$  on  $80^\circ$  pad.

An additional benefit of the  $44^\circ$  pivot position is an increase in the load capacity of the pad for a given eccentricity ratio or minimum film thickness. This is shown in Figure 2-7 in which the loads for a  $40^\circ$  and a  $45^\circ$  pivot position are plotted. The increase of the  $45^\circ$  over the  $40^\circ$  condition is 20% or more over the range shown. This data was obtained by placing the flexure pivot at the  $180^\circ$  position and finding the inlet angle which would generate a moment equivalent to a 2,000 in.-lb/rad flexure in the manner shown earlier.

### 2.1.4 The Assembled Four-Pad Bearing

MTI CADENSE 41\* is capable of analyzing a multiple-pad bearing in which the pivots are mounted on supports having a specified radial stiffness and is used for analyzing the complete bearing. No angular stiffness is accounted for, but the analysis of the single pad indicates that this will have only a very minor effect on bearing performance, particularly at the higher eccentricity ratios involved when a preload ratio of 0.65 is used. While thermal effects can also be introduced, we elected to run the program isothermally. This was later shown to be reasonable in view of the low temperature rises measured even at speeds as high as 30,000 r/min.

\*CAD-41 = Design of Gas-Lubricated Tilting Pad Bearings.

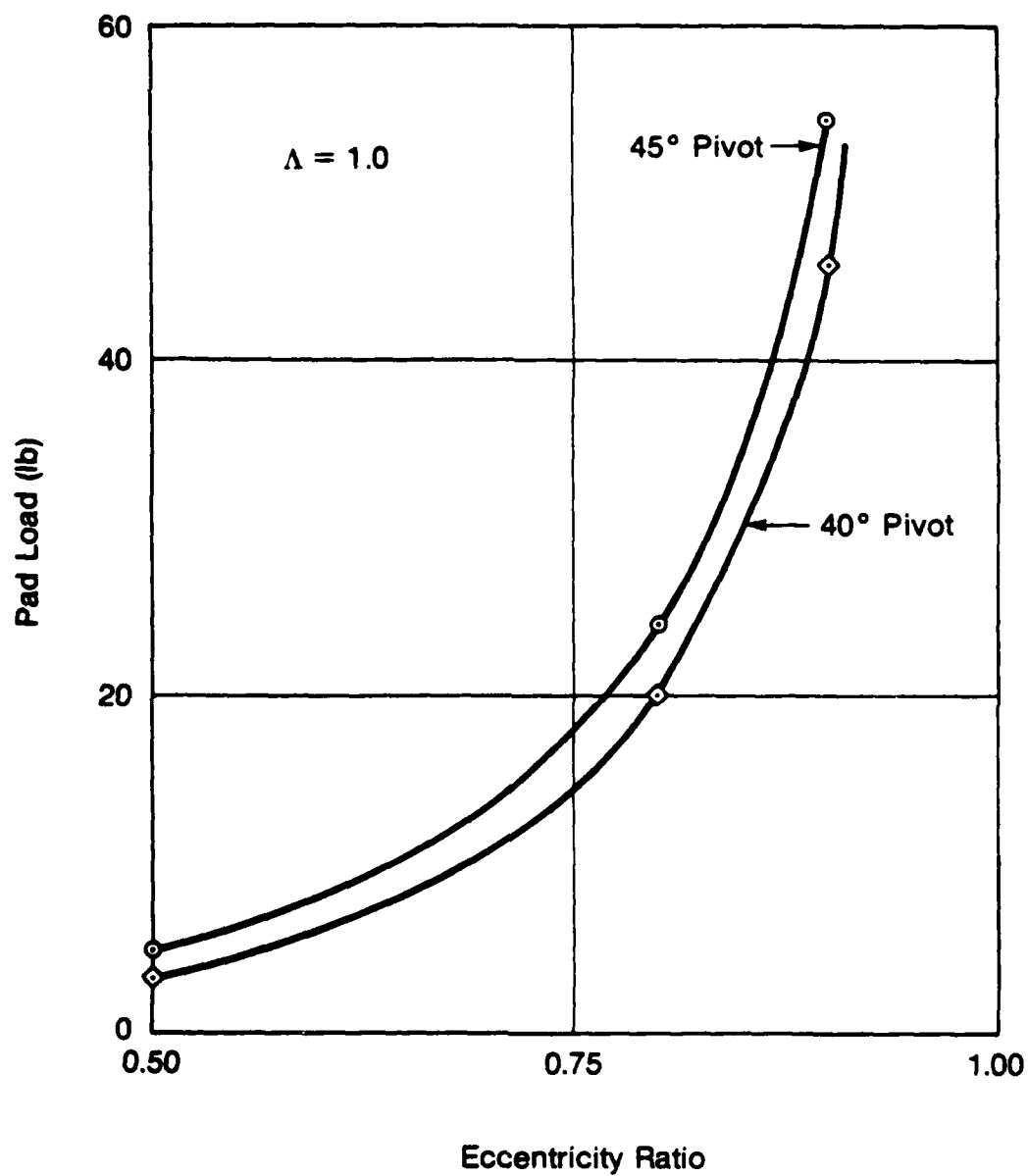


Fig. 2-7 Pad Load vs Eccentricity Ratio for 40° and 45° Pivot Position for a 2000 in.-lb/rad Flexure

The program was run in a mode in which the geometry, the load and the speed were specified and complete data on the static and dynamic performance were calculated. For the assembled bearing, the eccentricity, the horsepower loss, the four stiffness coefficients, and the four damping coefficients were calculated. Additional output included data for each individual pad, including pad load, film thickness at the pivot, the eccentricity ratio, the power loss, and the stiffness and damping coefficients.

The predicted performance is shown in Table 2-3 for the assembled four-pad bearing. The pivot locations are at 45, 135, 225 and 315° and so a vertical load is carried by two lower pads. Each pad is carried on a flexure providing a radial stiffness of 6,600 lb/in. At a preload ratio of 0.65, the centered shaft (zero load) clearance over each pivot is 0.0012 in. A vertical load from the rotor of 11.0 lb is assumed. Results are shown for speeds of 2,000, 5,000, 10,000, 20,000 and 30,000 r/min.

There are three groups of entries in Table 2-3, one for the bearing parameters, one for the upper pad parameters, and one for the lower pad parameters. Examining the bearing parameters first at  $\Lambda$  values based on the viscosity of air at an ambient temperature of 200°F reveals the following:

- Eccentricity. The eccentricity is large (1.2 mils) at low speed (2,000 r/min). As the speed increases, the eccentricity decreases, as would be expected, to about 0.4 mils at 30,000 r/min.
- Power Loss. Power Loss expressed in horsepower is small, about 0.002 at 2,000 r/min, and increases about 100-fold to nearly 0.2 at 30,000 r/min. As shown in Figure 2-8, the log of power loss is linear with the log of speed, varying as the 1.73 power of speed. If the shaft were centered in the bearing, i.e., if there were zero applied load, the power loss would be expected to vary as the square of the speed at constant temperature conditions.
- Stiffness. The stiffness of the overall bearing is nearly constant at about 6,000 lb/in. It does increase slightly with speed with a maximum

TABLE 2-3

## PREDICTED PERFORMANCE OF FOUR-PAD HYDROFLEX BEARING

Component	Parameter	Speed (r/min), $\Lambda$				
		2000, 0.0641	5000, 0.1603	10,000, 0.321	20,000, 0.641	30,000, 0.962
Bearing	Eccentricity, mils	1.2	0.90	0.66	0.47	0.39
	Power Loss, hp	0.0018	0.0079	0.026	0.093	0.196
	Stiffness, lb/in.	5540	5970	6820	6450	3010
	Damping, lb-s/in.	2.7	2.3	1.6	0.6	0.3
Upper Pad	Load, lb	0.30	0.95	2.28	4.79	7.00
	Min. Film Thk., mils	1.55	1.42	1.34	1.31	1.31
	Pivot Film Thk., mils	2.08	1.86	1.69	1.56	1.50
	Attitude Angle, deg.	43.6	37.9	32.8	27.3	23.7
	Radial Damped Freq., r/min	38,200	42,100	50,000	65,100	74,700
	Pitch Damped Freq., r/min	8,050	15,400	23,800	32,600	38,100
Lower Pad	Load, lb	8.07	8.72	10.06	12.57	14.78
	Min. Film Thk., mils	0.27	0.48	0.66	0.80	0.87
	Pivot Film Thk., mils	0.37	0.59	0.76	0.89	0.95
	Attitude Angle, deg.	14.2	15.6	16.1	15.5	14.3
	Radial Damped Freq., r/min	129,500	110,000	110,000	113,900	109,500
	Pitch Damped Freq., r/min	58,100	54,700	54,200	56,200	57,900

Pivot angles = 45°, 135°, 225°, 315° (45° from leading edge of 80° pad)  
 Preload = 0.65, D = 3.5 in., L = 2 in., C = 0.0035 in., Load = 11.0 lb vert.,  
 Flexure Stiffness = 6600 lb/in.

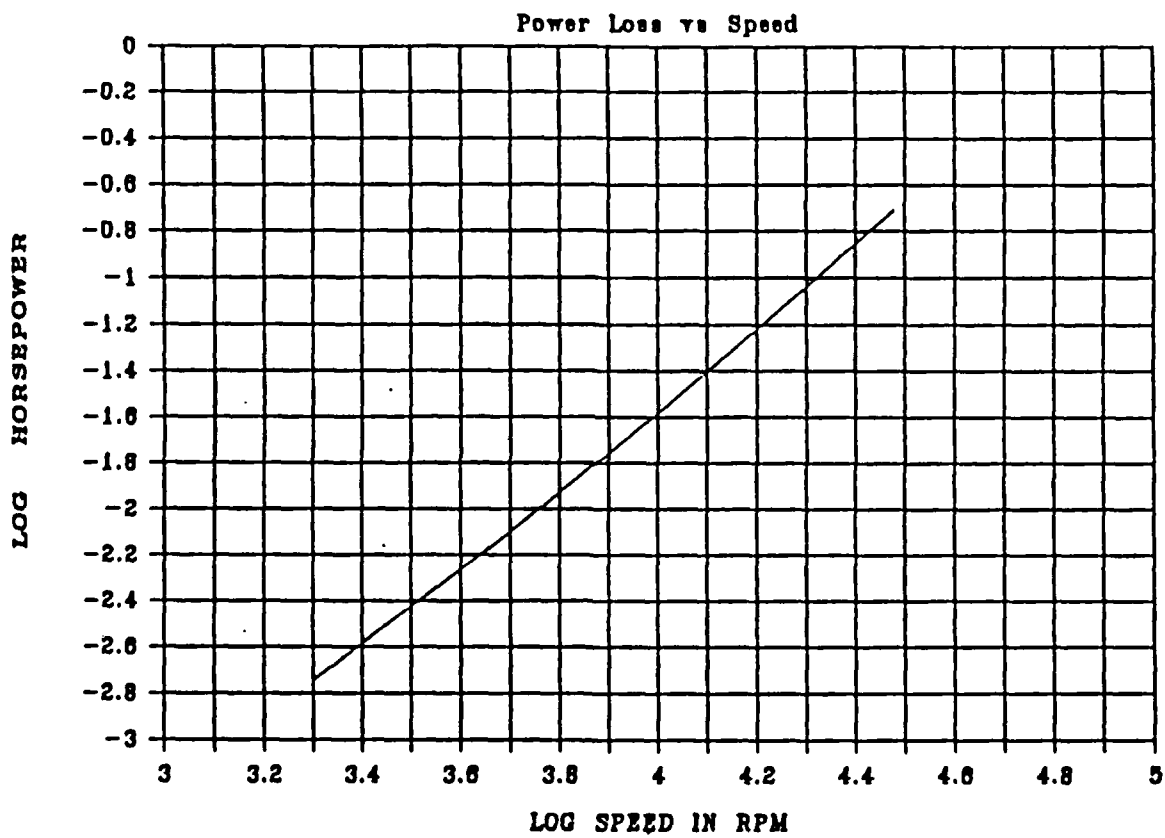


Fig. 2-8 Hydroflex Bearing

value at 10,000 r/min. Above 20,000 r/min, the stiffness drops rapidly to 3,000 lb/in. at 30,000 r/min.

- Damping. The level of damping is low, as would be expected in an air bearing, and drops as speed is increased. The damping values do not include any accounting for the Coulomb damping at the flexure that is an integral part of the overall design.

The second section of Table 2-3 shows the predicted performance of the upper pads, on a per pad basis.

- Pad Load. The load on the upper pad is low, but positive (due to the preload) at 2,000 r/min. It increases rapidly with speed as the shaft rises in the bearing.
- Film Thickness. The pivot film thickness decreases over the speed range from 2.1 mils to 1.5 mils. Correspondingly, the minimum film thickness located beyond the pivot at the line of centers decreases from 1.6 to 1.3 mils.
- Attitude Angle. The attitude angle of the upper pad is large,  $43.6^\circ$  at 2,000 r/min, and decreases steadily to  $23.7^\circ$  at 30,000 r/min, in a manner consistent with the increase in pad load.
- Damping Frequencies. The radial damped frequency is above the top speed range over the entire speed range. The damped frequency for pitch motion of the pad is lower, but is above the running speed over the entire speed range.

The final section of Table 2-3 presents the operating parameters for the lower pads, the results for one of the two equivalent lower pads being presented.

- Load. The load on each lower pad increases from 8.1 lb at 2,000 r/min to 14.8 lb at 30,000 r/min. The difference between the lower pad load and the upper pad load, multiplied by two and by the cosine of  $45^\circ$ , equals 11.0 lb. Thus, as the shaft rises in the bearing with increases



in speed, all pads carry more load, some of which is internally balanced.

- Film Thickness. The predicted film thicknesses at 2,000 r/min, only slightly above the observed liftoff speed of about 1,000 r/min, are a substantial 0.3 mils, a reasonable value for a gas bearing. This increases to about 0.9 mils at 30,000 r/min.
- Attitude Angle. The attitude angle increases slightly up to 10,000 r/min and then decreases to the top speed.
- Damped Frequencies. The damped natural frequencies for the lower pads, for both radial and pitch vibration, are far above the running speed range in all cases.

Another point that needs to be examined is the bearing behavior when higher loads are imposed. This is a condition that may be experienced due to shock, vibration, or the development of some degree of unbalance in the rotor. Table 2-4 summarizes the predicted film thicknesses over the loaded pad pivots and the horsepower loss over the range of loads from 11 lb to 140 lb at speeds of 10,000, 20,000 and 30,000 r/min. It is evident that, at 140 lb, film thicknesses of the order of only 0.1 mil are predicted, and hence continued operation at loads higher than 140 lb might be difficult. The power loss roughly doubles as the load is increased 13-fold from the design load of 11 lb to 140 lb.

The total shaft deflection, of course, increases as large loads are applied. This behavior is shown in Table 2-5 as a function of speed. In general, the eccentricity of the shaft is lower at the higher speeds. Note also that at the design preload of 0.65 there is still a small load on the upper pads over the speed range shown.

### **2.1.5 Unbalance Behavior**

In the test evaluation program, unbalance moments totaling as high as 0.002 in.-lb (600 mg at a radius of 1.5 in.) were applied at the test end of the

**TABLE 2-4**

**PREDICTED HYDROFLEX™ PERFORMANCE VERSUS LOAD**

Load (lb)	Pivot Film Thickness (mils)			Horsepower Loss		
	10,000 r/min	20,000 r/min	30,000 r/min	10,000 r/min	20,000 r/min	30,000 r/min
11	0.76	0.89	0.95	0.026	0.093	0.196
17	0.63	0.77	0.83	0.029	0.100	0.210
50	0.31	0.41	0.48	0.040	0.133	0.286
70	0.23	0.30	0.35	0.047	0.147	0.322
140	0.09	0.08	0.11	0.063	0.180	0.411

**TABLE 2-5**

**PREDICTED ECCENTRICITY VERSUS LOAD FOR HYDROFLEX™ BEARING**

Load (lb)	Eccentricity at Indicated Speed (MILS)		
	10,000 r/min	20,000 r/min	30,000 r/min
11	0.66	0.47	0.39
17	0.84	0.65	0.55
50	1.30	1.15	1.06
70	1.41	1.31	1.23
140	1.61	1.62	1.57

rotor. This amount of unbalance was run very successfully up to 30,000 r/min with no indication that this was a limiting condition.

If the shaft were running about its geometric center, this would be the equivalent of a centrifugal load of 50.6 lb. However, since this speed is far above the critical speed (approximately 6,000 r/min), the rotor runs about its mass center. This results in a shaft eccentricity of 0.194 mils. At the bearing stiffness of 3,010 lb/in., this is equivalent to a load change of 0.58 lb.

## 2.2 Flexure Design

The flexure design encompasses both the calculation of the flexure radial and moment stiffnesses and the mechanical design for fitting it into the bearing structure. The latter includes the design of the Coulomb dampers. Only the prediction of the stiffnesses is treated here.

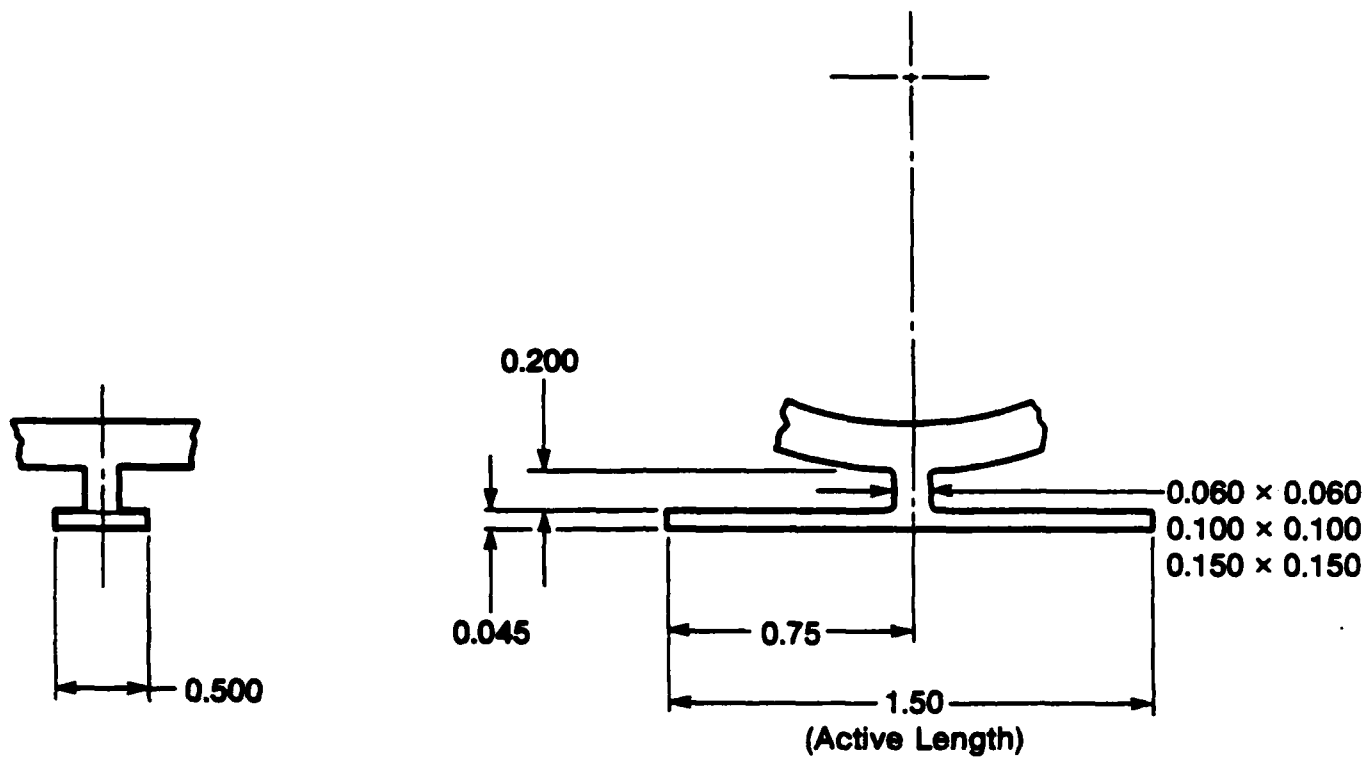
The radial and angular stiffnesses of the flexure were calculated using MTI finite-element programs PN1009A and B\*. A typical Hydroflex flexure design is shown in Figure 2-9. A finite-element model of the structure is shown in Figure 2-10. Three cases were studied with different sizes of the center post. These are:

Case Number	Size of Center Post (in.)
1	0.060 x 0.060 x 0.200
2	0.100 x 0.100 x 0.200
3	0.150 x 0.150 x 0.200

Radial stiffness was obtained by assuming a radial force to be applied at the center of the horizontal beam member and calculating the deflection at the bottom center of the beam. Using a force of 10 lb, and a beam cross-section of 0.045 x 0.500 in., the deflection was calculated to be 0.00145. This gives a stiffness of 10/0.00145, or 6,900 lb/in.

---

\*PN1009A = Two-Dimensional Mesh Generator and PN1009B = Two-Dimensional Stress Analysis for PN1009A.



Dimensions in inches

Fig. 2-9 Hydroflex<sup>TM</sup> Bearing Flexure Design

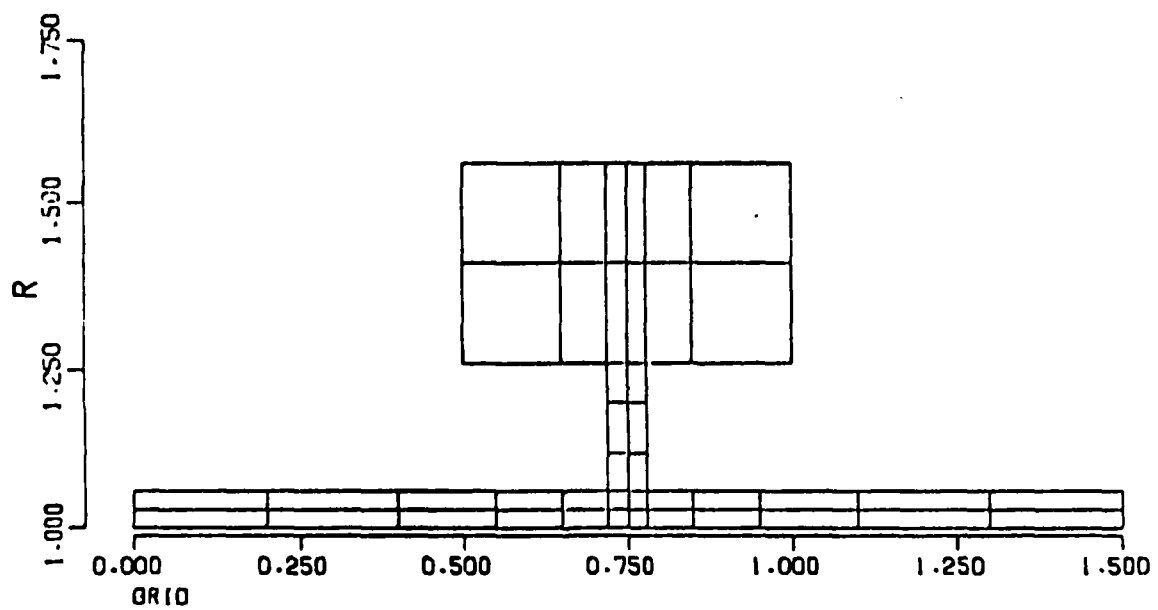


Fig. 2-10 Analytical Model of Flexure Pad Support

The angular stiffness was calculated by applying a force couple to the bearing pad and determining the bending of the post and the bending of the flexure beam that results. The results are as follows:

Case No.	Center Post Size	Total Stiffness ( $K\xi$ )
1	0.06	303
2	0.10	1388
3	0.15	2907

where  $K\xi$  is the angular stiffness in in.-lb/rad, and the values for both the post alone and the total including the flexure beam are given. As a result of these calculations, the heavier post cross-section was deemed to be adequate for pad flexibility and to provide a more rugged construction.

### 3.0 TEST VEHICLE DESIGN

The test vehicle design for evaluating the Hydroflex™ bearing concept incorporates a ball-bearing support in conjunction with the Hydroflex bearing as shown in Figure 3-1. In this figure can be located the Hydroflex bearing assembly, (1), the test rotor, (2), the duplex ball bearing pair, (3), and the drive turbine, (4).

Several additional features have been incorporated into the tester design, including the following:

- Reversing turbine buckets (5) to provide rapid deceleration of the rotor shaft, if required.
- Precision spacers (6) for accurately locating the Hydroflex bearing housing (7) to the support bearing housing (8).
- A turbine nozzle and manifold box (9) for improving the drive turbine efficiency.

Instrumentation provided for the Hydroflex tester includes the following:

- Capacitance probes (10), positioned in a vertical and horizontal orientation at both support bearing locations, which are used to measure rotor excursions.
- Magnetic pickup (11) for monitoring rotor rotational speed.
- Eddy current probes (12) positioned to monitor the radial and pitching motion of a single Hydroflex pad.
- Thermocouples positioned in each Hydroflex bearing pad for monitoring pad temperature. The thermocouples are located at the Hydroflex pad center plane, 3/16 in. inboard of the trailing edge and within 0.06 in. of the pad's active surface. Thermocouple locations are illustrated in Figure 3-2.

A schematic of the instrumentation system is shown in Figure 3-3.

A critical speed calculation, based on the rotor model illustrated in Figure 3-4 was used for determining the number, the speed and the mode shapes of the

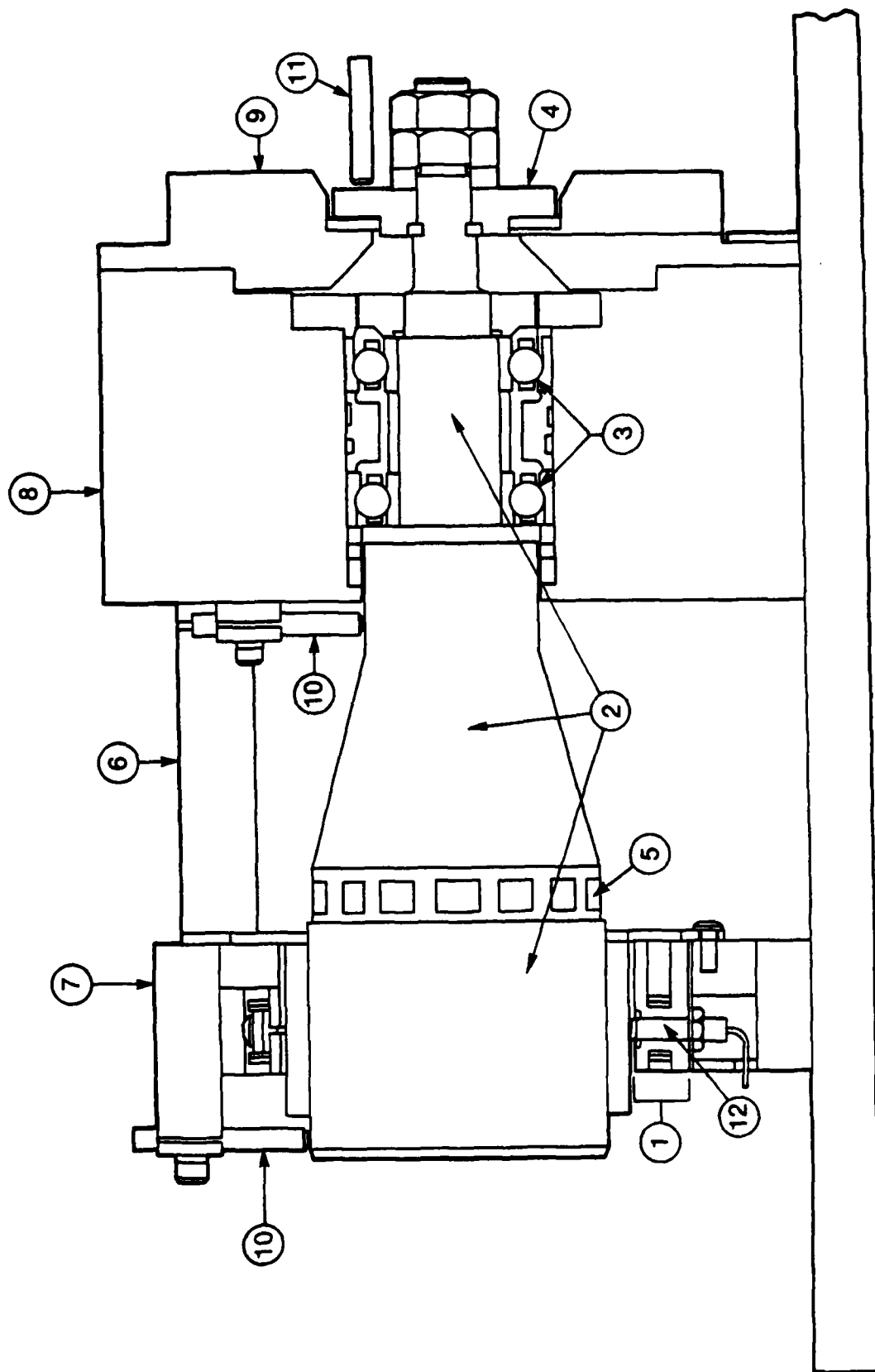


Fig. 3-1 Hydroflex™ Bearing Test Vehicle



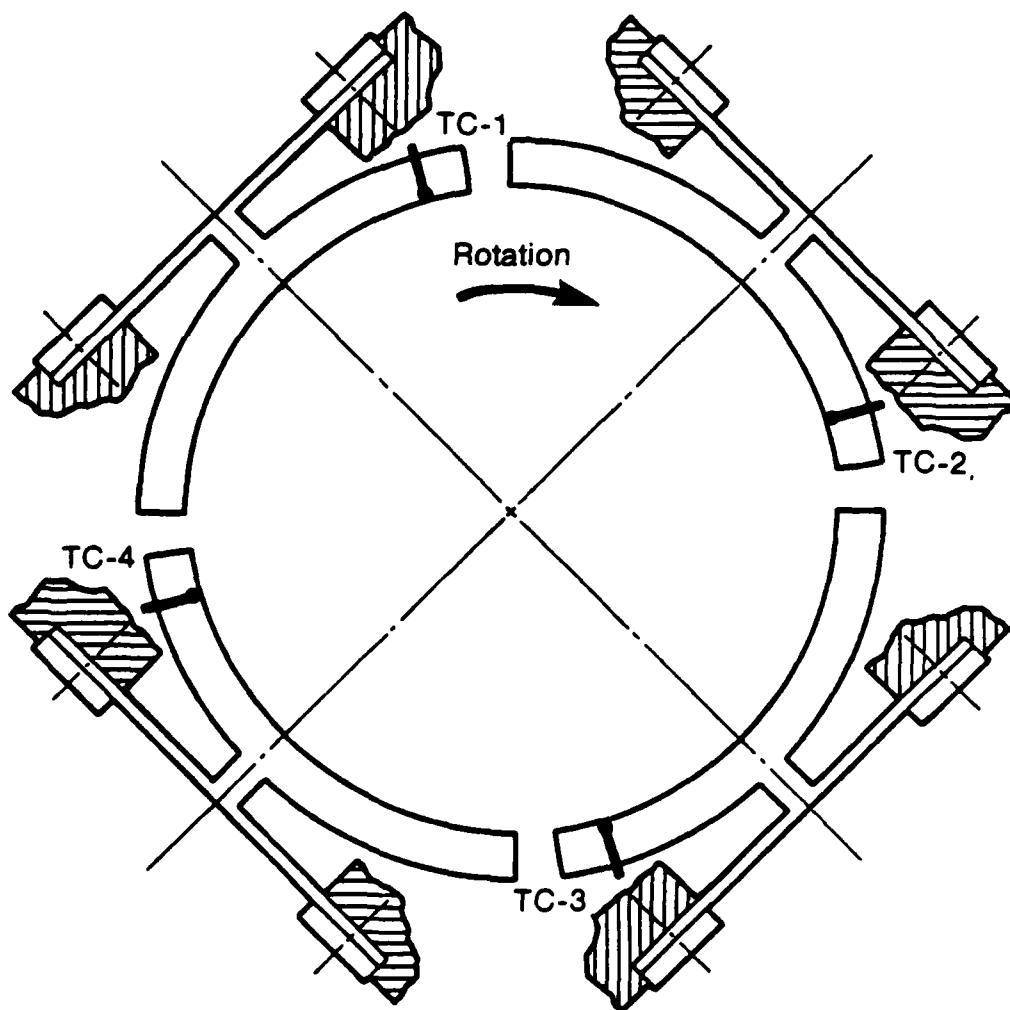


Fig. 3-2 Hydroflex<sup>TM</sup> Bearing Pad Thermocouple Orientation

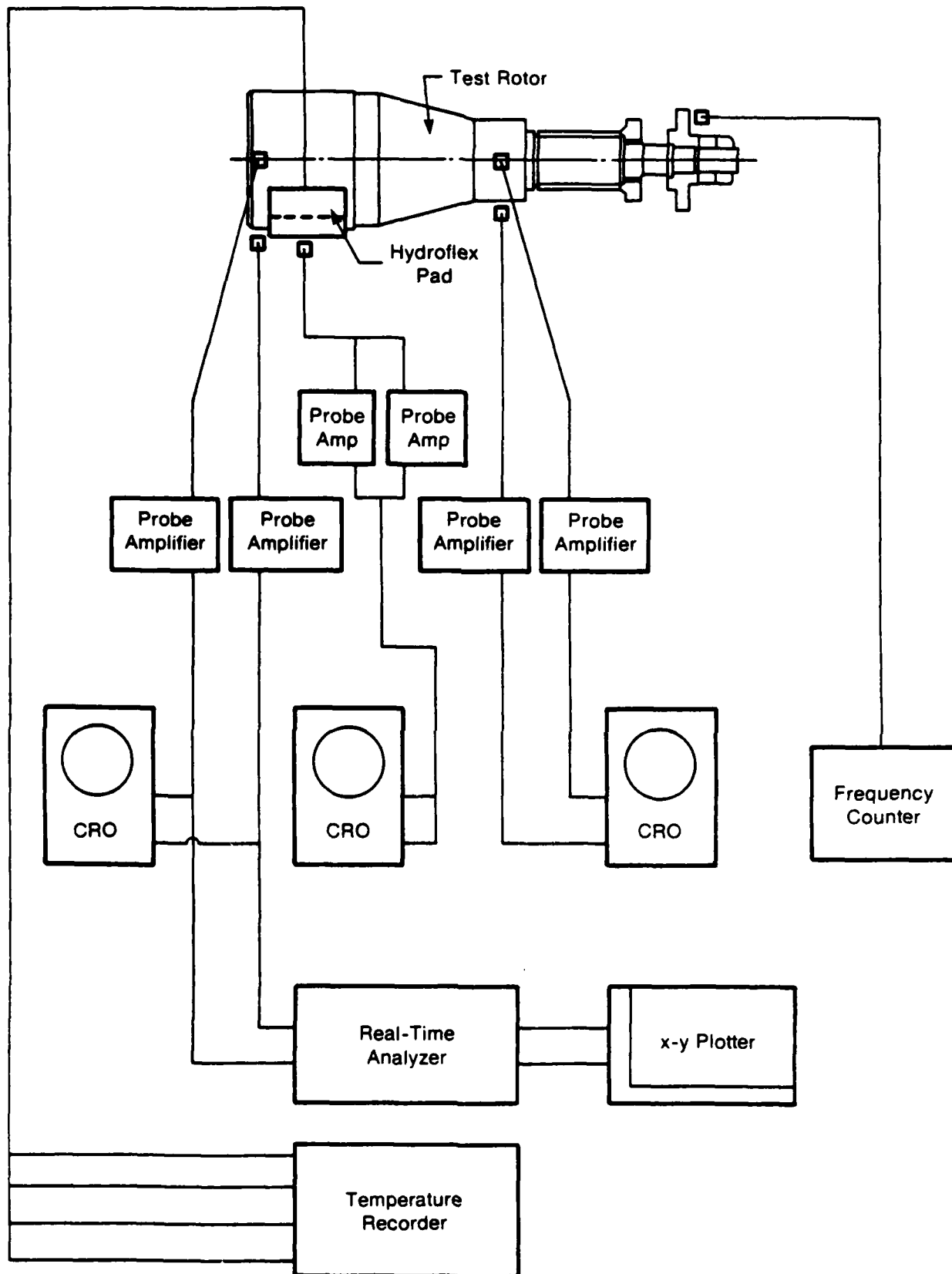


Fig. 3-3 Instrumentation Schematic

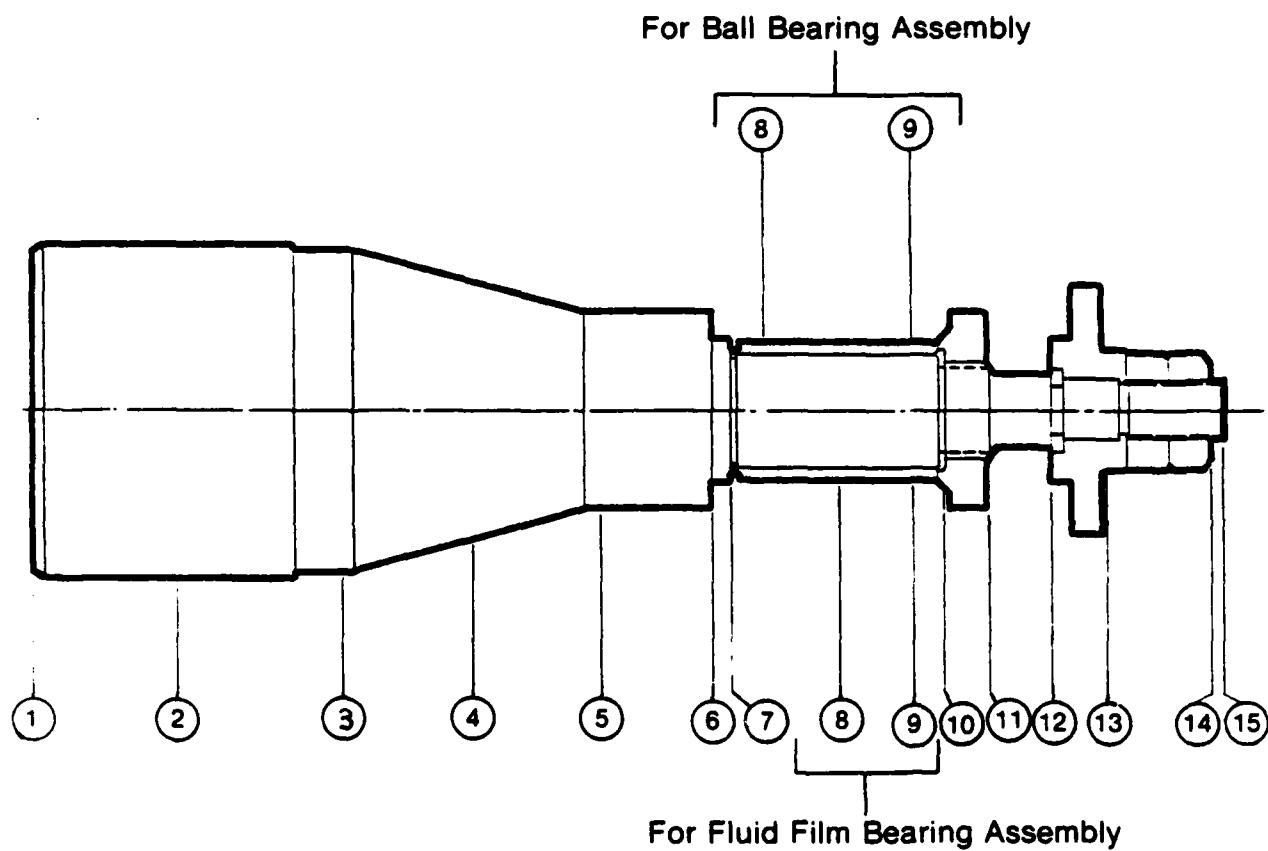


Fig. 3-4 Rotordynamic Model

test rotor critical speeds. Those critical speeds which fall below the maximum target speed of 30,000 r/min would have to be crossed during execution of the program test plan.

The critical speed map, calculated at a fixed ball-bearing stiffness of  $K = 10^6$  lb/in. at each bearing location (Stations 8 and 9 for the ball-bearing assembly on Figure 3-4) is presented in Figure 3-5 which shows the rotor critical speeds as affected by a variation of Hydroflex bearing stiffness (also as a function of speed). Table 3-1 lists several rotor speeds, the associated bearing stiffnesses, and the critical speeds corresponding to those stiffnesses.

The table of critical speeds, using calculated Hydroflex bearing stiffnesses and the data from Figure 3-5 show that only one critical speed at 8,800 r/min exists below the maximum desired test speed of 30,000 r/min. The mode shape for the lowest critical speed is conical with the cone apex midway between the two ball bearings, thereby providing the necessary rotor response amplitude at the Hydroflex bearing for evaluation of external damping effectiveness.

The acceptable, analytically derived performance of the Hydroflex tester design permitted its parts detailing and fabrication. A photograph of the finished rotor assembly is shown in Figure 3-6; a Hydroflex pad photograph, in Figure 3-7. Individual Hydroflex bearing pads were machined from single blocks of through-hardened tool steel by the wire EDM process. The entire pad profile, including the flexure and active bearing surface, was machined in one continuous pass.

Two secondary operations, also performed by the EDM process, were to undercut the pad center post in the orthogonal plane from the contour cut and to provide the bolt holes in the flexure. Aside from a process to apply a protective, solid-lubricant film coating to the bearing pads, no additional machining operations were required prior to placing the pads into service.

The four Hydroflex pads making up a Hydroflex bearing are shown assembled into their mounting frame in Figure 3-8. The fully assembled tester is illustrated in the photograph presented in Figure 3-9.

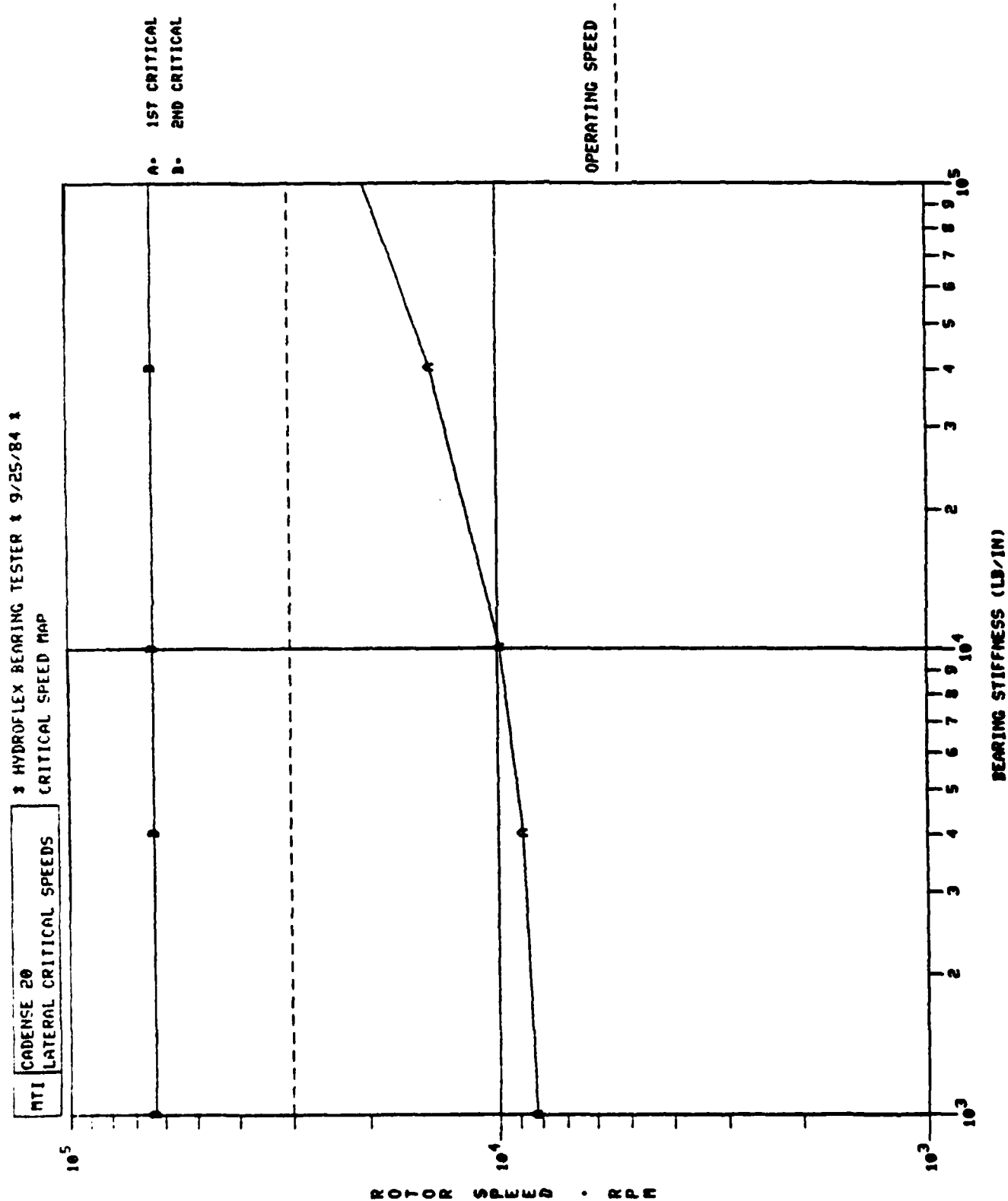


Fig. 3-5 Critical Speed Map - Hydroflex<sup>TM</sup> Bearing Tester - Ball Bearing Assembly

TABLE 3-1  
HYDROFLEX<sup>TM</sup> STIFFNESS - CRITICAL SPEED RELATIONSHIP  
BALL BEARING DESIGN

Rotor Speed (r/min)	Hydroflex Stiffness (lb/in.)	Critical Speed (r/min)	
		1st	2nd
2,000	$5.54 \times 10^3$	8,780	63,212
5,000	$5.97 \times 10^3$	8,780	63,212
10,000	$6.52 \times 10^3$	8,800	63,212
20,000	$6.45 \times 10^3$	8,800	63,212
30,000	$3.01 \times 10^3$	8,600	63,212

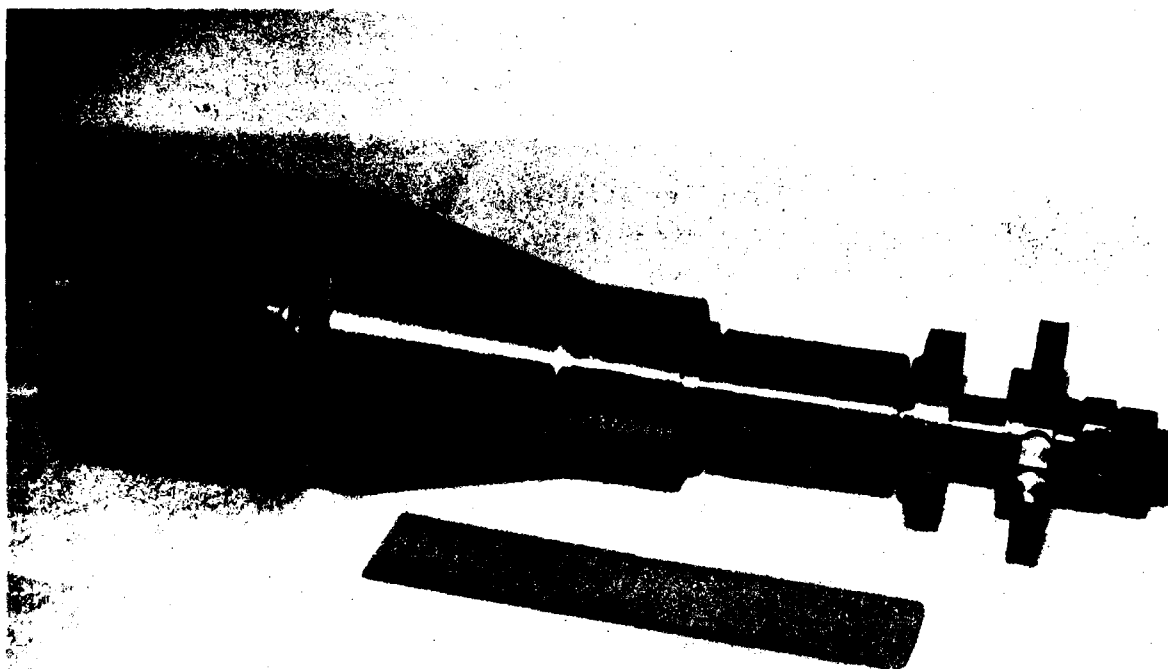


Fig. 3-6 Test Rotor Assembly



Fig. 3-7 Hydroflex<sup>TM</sup> Bearing Pad



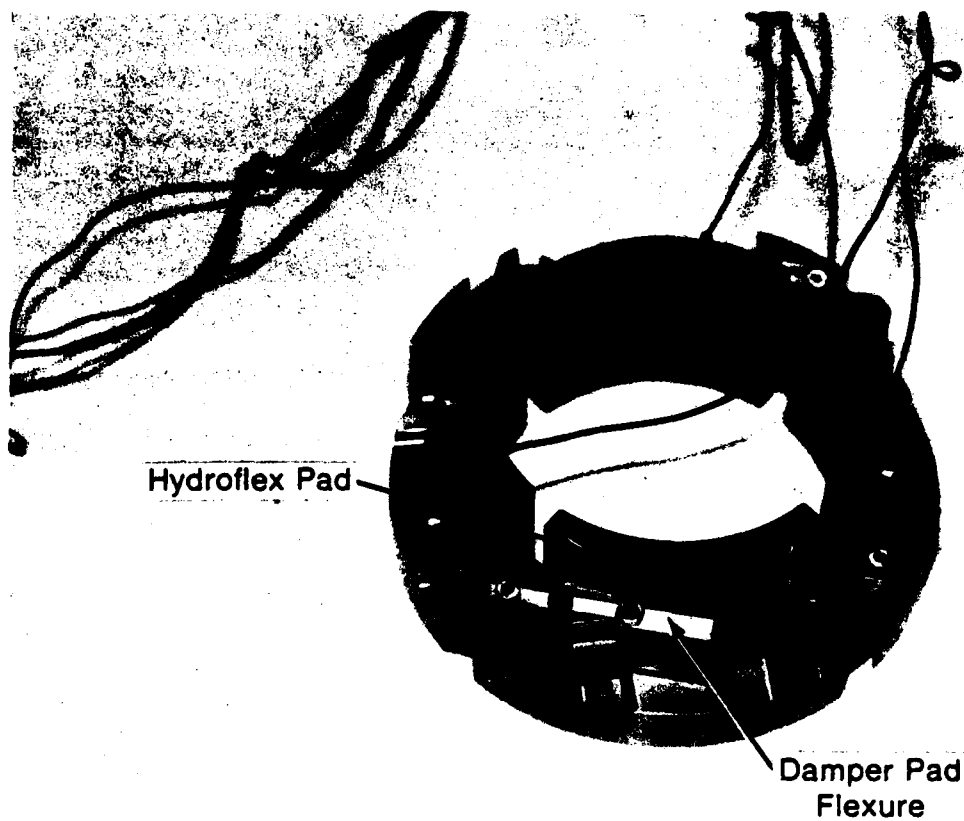


Fig. 3-8 Hydroflex™ Bearing Assembly

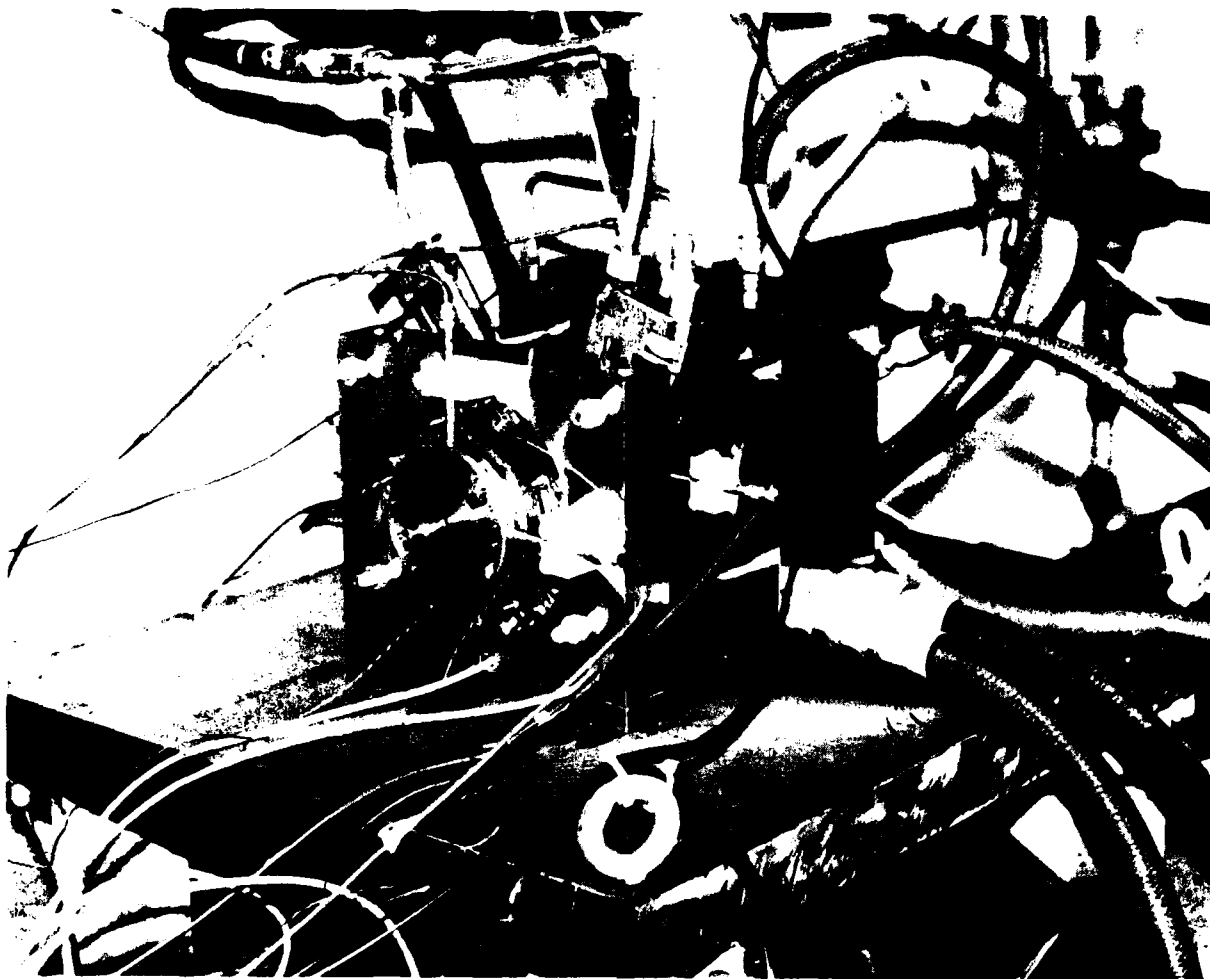


Fig. 3-9 Hydroflex<sup>TM</sup> Test Apparatus

After assembly, an operational checkout of the ball-bearing-supported tester configuration showed the expected rotor response at the Hydroflex bearing, but the magnitude of the response and the location of the peak amplitude were somewhat surprising. The experimental response curves presented in Figure 3-10 include a damped response for the Hydroflex bearing, with the horizontal response approaching a peak at rotor speeds near 11,000 r/min. For reference, this double amplitude at the peak horizontal replacement corresponds to a rotor excursion of 0.0036 in., more than 0.001 greater than the static clearance. Although a dissymmetry across pairs of Hydroflex bearing pads causes a speed difference between the maximum vertical and horizontal amplitudes, the response curves, which show a 20% amplitude reduction when comparing damped to undamped data at 10,000 r/min, indicate that external friction damping is effective. Even with external damping, the high-speed rotor response at the Hydroflex bearing was sufficient to prevent a safe transition through the critical. The inability to traverse the first critical speed as a result of the excessive response amplitude at the maximum test speed prompted an in-depth examination of the tester to determine the reason for the difficulty.

A thorough examination of the tester assembly and its performance produced the following results:

1. The apparent location of the first critical speed near 11,000 r/min indicates that the ball bearings have a much higher stiffness than anticipated.
2. A very low-speed (less than 100 r/min) dynamic orbit of  $7 \times 10^{-4}$  in., peak-to-peak, was present at the Hydroflex bearing, although the measured out-of-roundness of the Hydroflex journal was only  $1 \times 10^{-4}$  in.
3. The apparent cause of this low-speed dynamic orbit was a non-parallel orientation of the two ball-bearing inner races. Because of the ratio of the ball bearing center distance (1.58 in.) to the center distance from the ball bearing set to the Hydroflex bearing (7.00 in.), an out-of-parallel condition of only  $1.6 \times 10^{-4}$  in. at the ball-bearing inner races is all that was needed to produce the

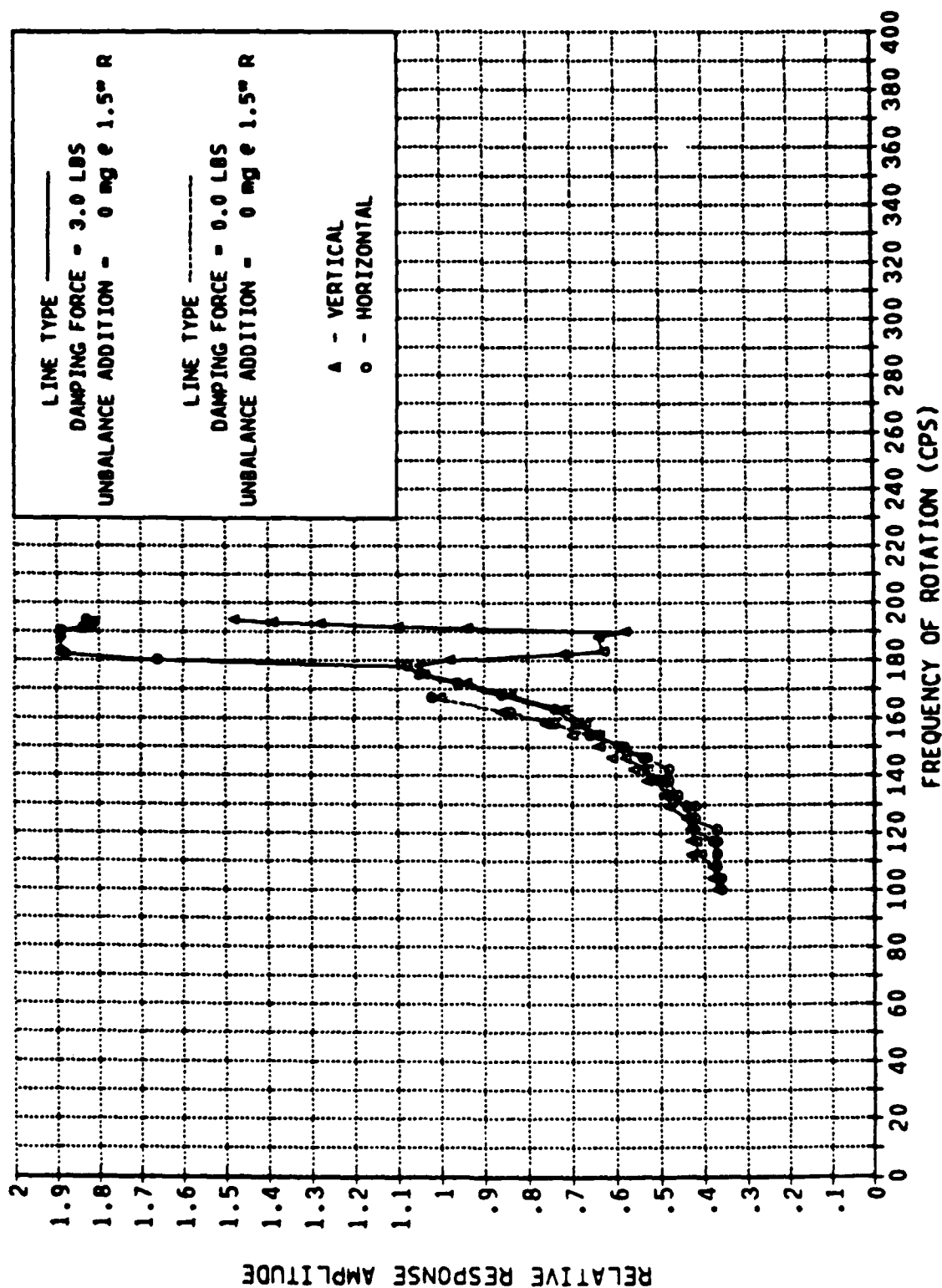


Fig. 3-10 Experimental Response Curve - Ball Bearing Assembly



Clearance	Eccentricity	Average Temp. (°F)
0.001	0.666	197.4
0.0015	0.740	162.6
0.002	0.792	144.2

The 0.001-in. clearance was rejected because of the higher average temperature. The 0.002-in. clearance was also rejected because of very high eccentricity values at and below 5,000 r/min. The 0.0015-in. clearance was then selected and examined over the entire speed range. The operating results calculated are presented in Table 3-2. The eccentricity ratio of 0.74 at 30,000 r/min indicated that this bearing should operate up to this speed in a dynamically stable regime. The operation during the test program confirmed this view.

The introduction of the fluid film bearing, with a much lower radial stiffness and no angular stiffness, provided two benefits; one was the lowering of the first critical speed, the second, the elimination of the dynamic runout which forced high response amplitudes at the original critical speed.

A critical speed calculation based on the rotor model illustrated in Figure 3-4 for the fluid film bearing assembly was performed resulting in the representative critical speed map is shown in Figure 3-11. Table 3-3 shows the new critical speeds corresponding to the Hydroflex stiffness originally presented in Table 3-1. As a further aid in evaluating test results, a rotor response calculation based on calculated stiffness and internal damping coefficients for both the Hydroflex and the fluid film bearing was performed. The results of this calculation are presented in Figures 3-12 and 3-13 for the identified rotor stations. The unbalance of  $1.0 \times 10^{-3}$  in.-oz. located only in Station 1 is three times the actual residual unbalance of the present rotor assembly. The response calculation assumes the entire rotor, except for the unbalance input, is in perfect balance. From the calculated response results, it is obvious that only the first critical speed, at approximately 4,000 r/min, shows an amplitude peak and that its maximum 1/2 amplitude is less than  $50 \times 10^{-6}$  in. This low response is important since it provides ample margin for exploration of unbalance response and the effectiveness of the externally applied Coulomb damping.

TABLE 3-2

CALCULATED DATA FOR OIL-LUBRICATED SUPPORT BEARING

Speed (r/min)	Eccentricity	Attitude Angle	Horsepower	Flow (g/min)	Average Temperature ( F)
500	0.987	14.0	0.0005	0.0016	104.6
1,000	0.969	17.4	0.0014	0.0030	106.6
2,000	0.954	19.8	0.0046	0.0056	111.7
4,000	0.905	24.4	0.0123	0.0103	117.1
6,000	0.878	26.9	0.0234	0.0146	122.9
10,000	0.835	29.7	0.0499	0.0226	131.6
20,000	0.778	34.3	0.140	0.0403	149.5
30,000	0.740	36.4	0.248	0.0567	162.6

MTI CADENSE 20  
LATERAL CRITICAL SPEEDS

HYDROFLEX BEARING 2 4/30/85 2  
CRITICAL SPEED MAP

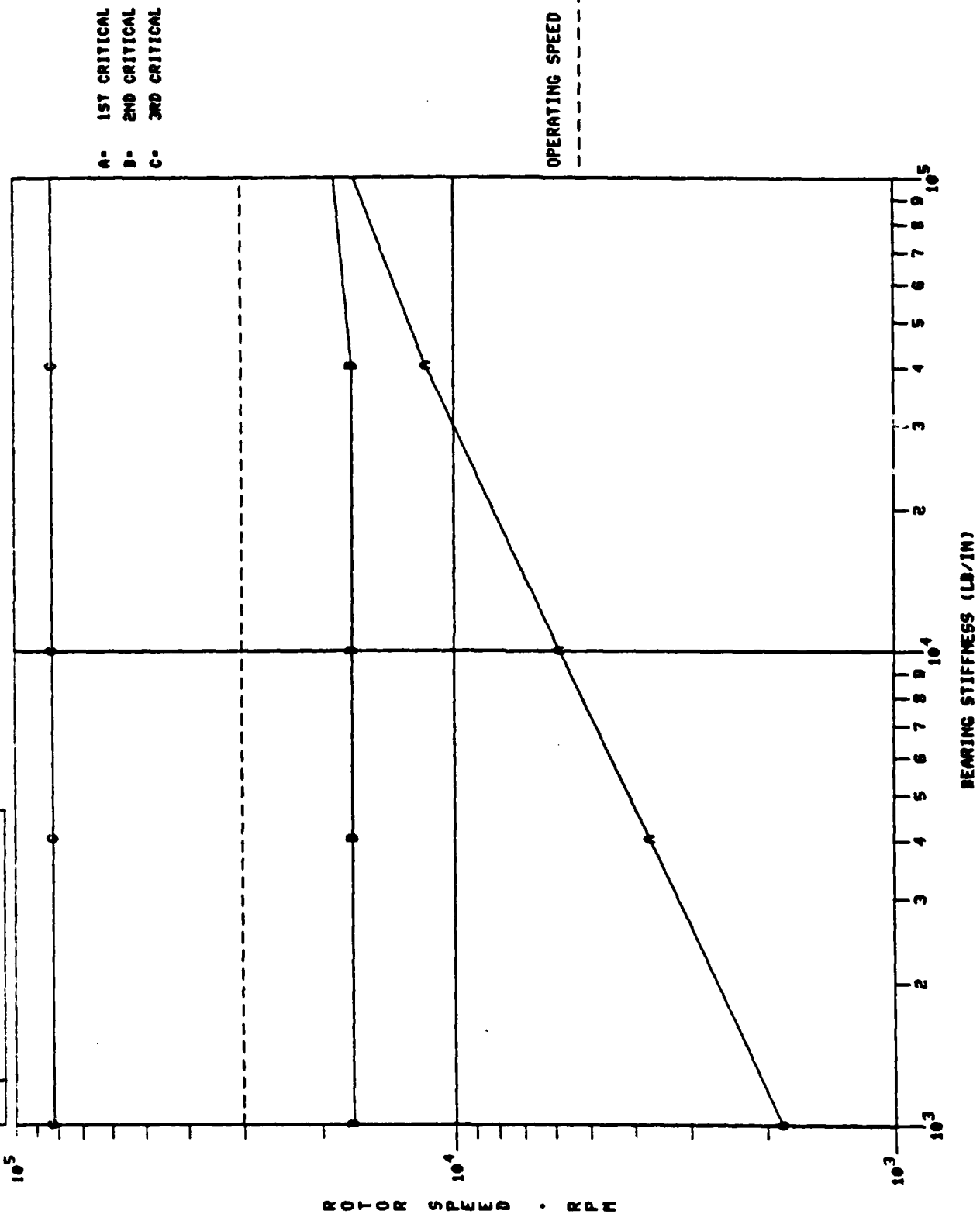


Fig. 3-11 Critical Speed Map - Hydroflex<sup>TM</sup> Bearing Tester - Fluid Film Bearing Assembly

852653



TABLE 3-3

HYDROFLEX<sup>TM</sup> STIFFNESS - CRITICAL SPEED RELATIONSHIP  
FLUID FILM BEARING DESIGN

Rotor Speed (r/min)	Hydroflex Stiffness (lb/in.)	Critical Speed (r/min)	
		1st	2nd
2,000	$5.54 \times 10^3$	4,200	16,960
5,000	$5.97 \times 10^3$	4,500	16,960
10,000	$6.92 \times 10^3$	4,800	16,960
20,000	$6.45 \times 10^3$	4,800	16,960
30,000	$3.01 \times 10^3$	3,200	16,960

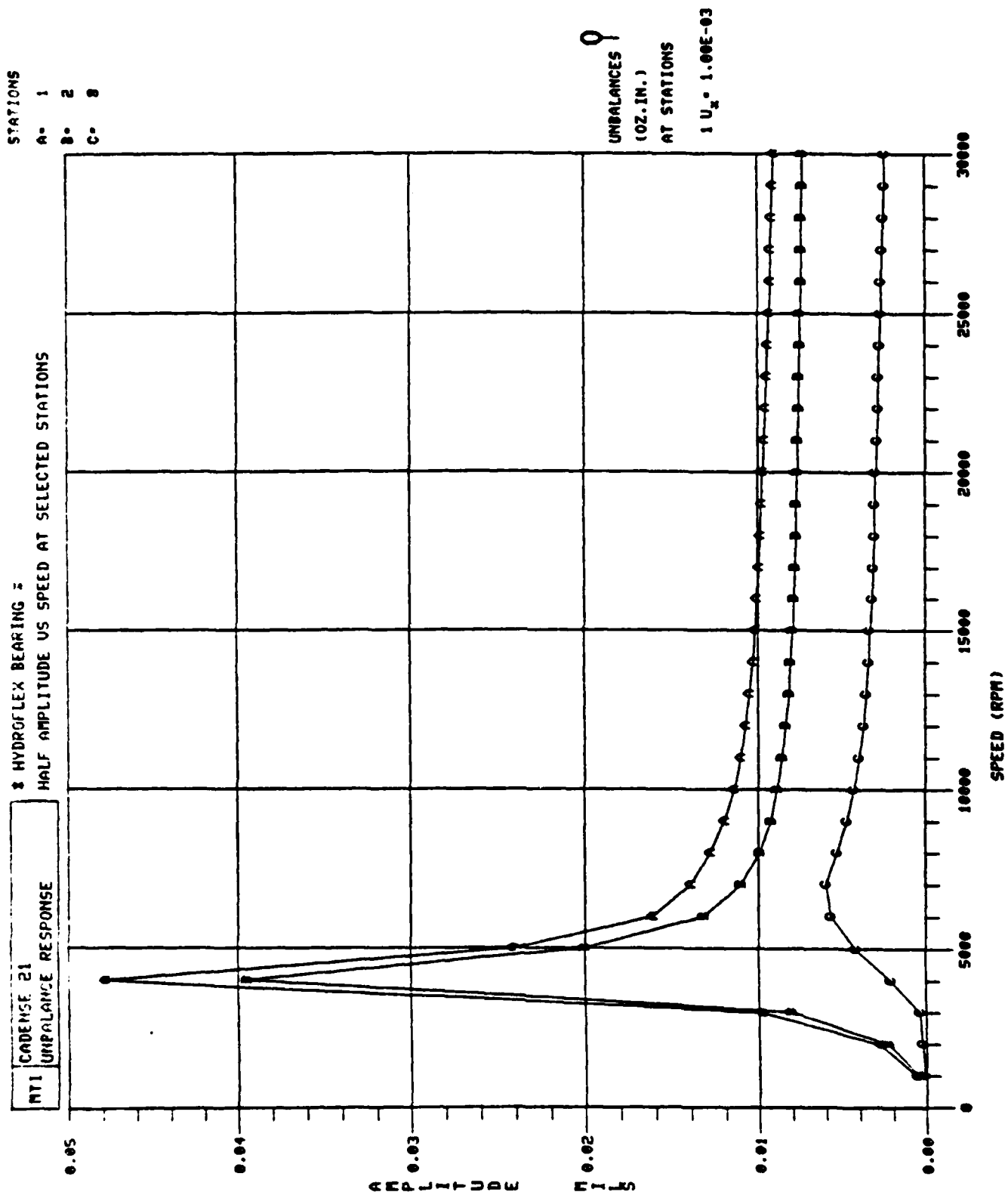


Fig. 3-12 Analytical Rotor Response - Fluid Film Bearing Assembly, Stations 1, 2, & 8

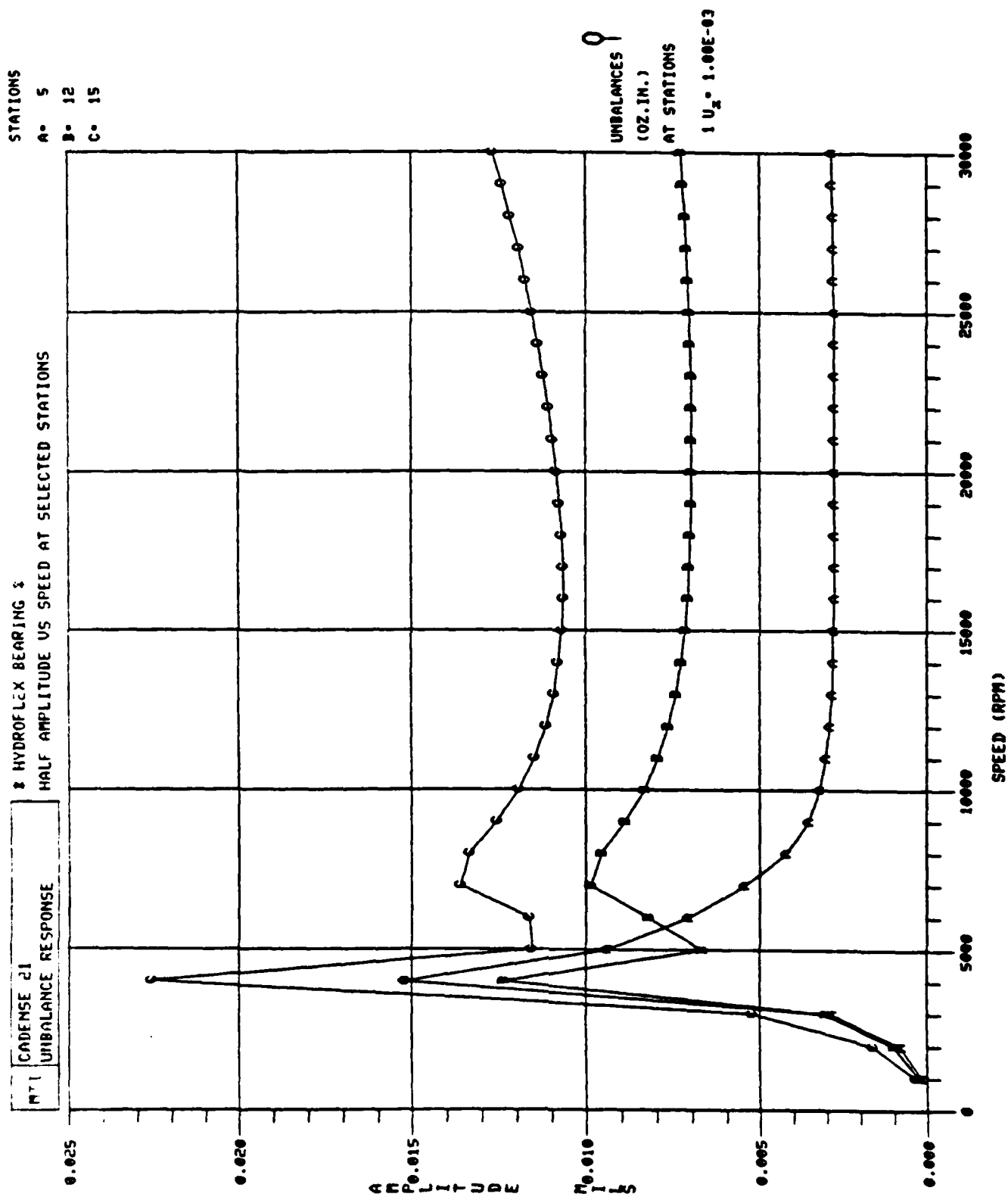


Fig. 3-13 Analytical Rotor Response - Fluid Film Bearing Assembly, Stations 5, 12, & 15

Two drawbacks result from the introduction of the fluid film bearing; one is the presence of a second critical speed (at 16,000 r/min) within the test plan speed range (Figures 3-12 and 3-13). This critical speed also takes a conical mode shape but with the cone apex at the Hydroflex bearing. The second drawback was disclosed when a bearing rotor system stability calculation showed that there was a log decrement sign change, indicating the possibility of bearing instability at speeds above 25,000 r/min.

Since the introduction of the fluid film bearing indicated a dramatic improvement in expected tester performance, the new design was implemented. After reassembly of the tester with the new bearing, a trial run was made up to a speed of 21,000 r/min, which is well past the critical speeds anticipated, confirming the redesign and permitting the implementation of the test program.

#### **4.0 EXPERIMENTAL EVALUATION OF THE HYDROFLEX BEARING**


The test program originally envisioned for evaluating the Hydroflex™ bearing and formalized into an approved test plan provided a systematic test sequence for evaluating the experimental behavior of the Hydroflex bearing design. The test program was divided into the following four tasks.

- Static measurement of both bearing pad and damper spring rates
- Dynamic evaluation of damping rates
- Dynamic evaluation of rotor response to varied levels of rotor unbalance
- Dynamic evaluation of rotor response to external excitation.

##### **4.1 Static Spring Rate Measurements**

Each of four Hydroflex bearing pads and the eight damper spring levers were measured to establish their spring rates. The Hydroflex pad spring rates, measured with the pads mounted in their usual way, were determined for three degrees of freedom, i.e., radial, pitch and roll. The damper springs were evaluated for bending stiffness only.

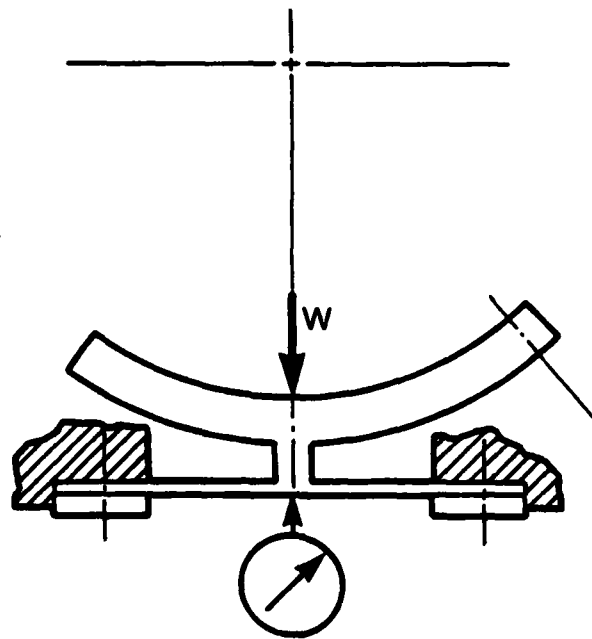
The test setups for these experiments are shown schematically in Figures 4-1 and 4-2.

For each spring rate test, several loads, ( $W$ ), were applied to the test specimens via a precision force gage. At each load, dial indicators, , were read to determine deflections. From these data and using appropriate geometric relationships, the slopes of the deflection curves, representing the static stiffness of the component measured, were determined.

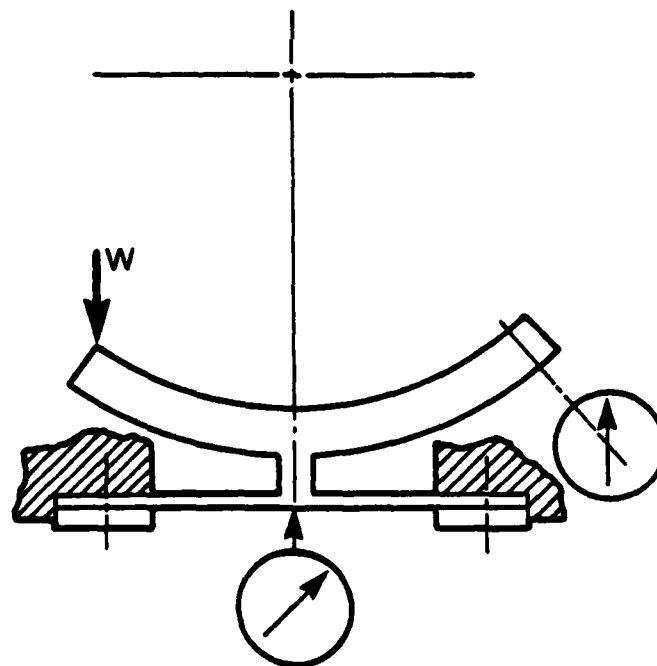
The results of the stiffness measurements are shown on Table 4-1.

##### **4.2 Dynamic Evaluation of Damping Rate and Rotor Unbalance Response**

The satisfactory modification to the tester permitted operational testing of the Hydroflex bearing at speeds well above the first rotor critical speed.

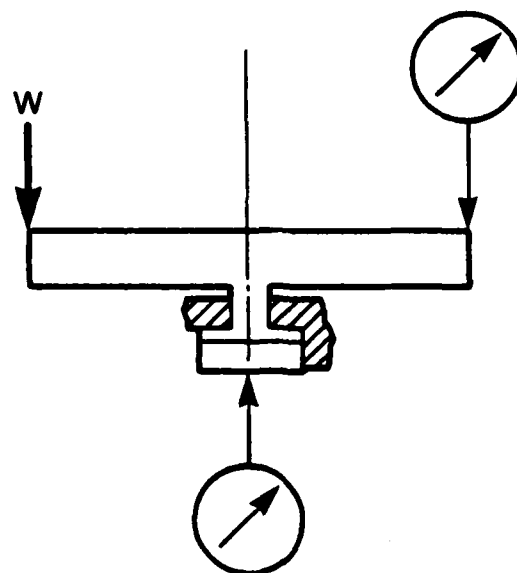


a. Radial Stiffness of Hydroflex™ Pad

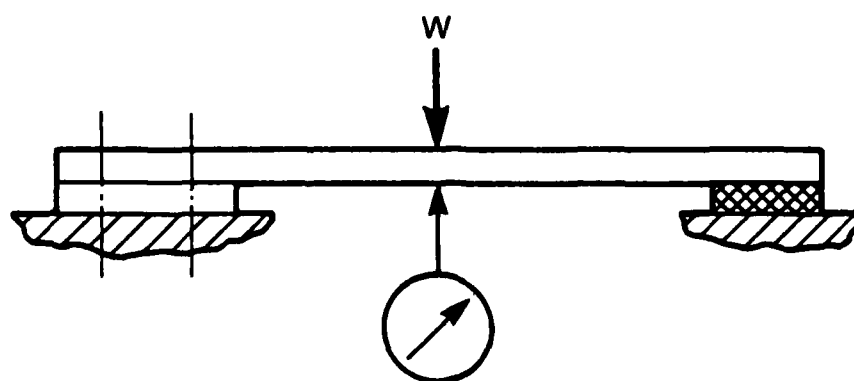


b. Pitch Stiffness of Hydroflex™ Pad

Fig. 4-1 Test Setup for Hydroflex™ Pad Stiffness Measurement



a. Roll Stiffness of Hydroflex<sup>TM</sup> Pad



b. Bending Stiffness of Damper Spring

Fig. 4-2 Test Setup - Hydroflex<sup>TM</sup> Bearing Component Stiffness Measurement

TABLE 4-1

MEASURED STIFFNESS - HYDROFLEX<sup>TM</sup> BEARING

Pad No.	Radial Stiffness (lb/in.)	Pitch Stiffness (10 <sup>3</sup> in.-lb/rad)	Roll Stiffness (10 <sup>2</sup> in.-lb/rad)
1	6190	2.11	5.73
2	7000	2.05	5.29
3	6000	2.10	7.16
4	6670	2.08	6.09
5	6460	1.98	5.73
6	6300	2.08	6.03
Calculated Value	6900	2.91	----

Average Damper Spring Stiffness. . . . . 7,500 lb/in.

TABLE 4-2

HYDROFLEX<sup>TM</sup> BEARING DYNAMIC TEST MATRIX

Data Point	Friction Damper Force (lb)	External Unbalance (in.-oz)	Assembly Type
1	0	0	Ball Brg.
2	3 lb., foam back*	0	↓
3	0	0	Fluid Film Brg.
4	0	4 x 10 <sup>-3</sup>	↓
5	0	8 x 10 <sup>-3</sup>	↓
6	0	16 x 10 <sup>-3</sup>	↓
7	0	32 x 10 <sup>-3</sup>	↓
8	3 lb., foam back*	0	↓
9	3 lb.	0	↓
10	↓	4 x 10 <sup>-3</sup>	↓
11	↓	8 x 10 <sup>-3</sup>	↓
12	↓	16 x 10 <sup>-3</sup>	↓
13	↓	32 x 10 <sup>-3</sup>	↓

\*Foam backing was a folded pad of EAR Corp. C-3003-7 energy absorbing foam placed behind pad flexures.



Successful testing was accomplished to speeds of 21,000 r/min (above the anticipated 2nd critical speed), but deviations from the test plan were necessitated by early test results.

The first deviation taken was with the method of determining the level of damping, i.e., the damping ratio  $B/B_c$ . The original plan called for determining the log decrement,  $\delta$ , by measuring successive peak displacements during vibration decay after striking the tester. The rapid vibration decay in only two or three cycles precluded any damping evaluation by this technique. It was decided to approximate the effectiveness of the external damping by measuring the Q factor of steady-state resonance at the first rotor critical speed. This method, which was successfully applied, is described in Section 5.0.

The second test plan deviation required limiting the amount of external damping that could be applied to the test bearing. The difficulty in applying several significant levels of damping load via the damper springs is that the higher damping loads would severely restrict the possible pad motion, thereby affecting bearing performance.

From Table 4-1, it can be seen that the nominal pad flexure radial spring rate is approximately  $6.4 \times 10^3$  lb/in. or 6.4 lb/mil. If a 6- or 7-lb damper friction force is applied against a Hydroflex pad, it is obvious that under conditions of high rotating loads, an individual pad could be forced radially outward and would not return to within a mil (0.001 in.) of its original setup position. This would cause a serious bearing malfunction. A judgment was made that a maximum safe damper friction force of 3 lb would be applied and that all testing with external damping would occur at this level.

With a satisfactory tester configuration and the procedure established for conducting a satisfactory test program, the evaluation of the Hydroflex bearing concept commenced. The test matrix listed in Table 4-2 was prepared and executed.

At each data point, covering a speed range extending to 21,000 r/min, the response amplitude at the Hydroflex bearing was recorded as a function of

rotor speed. Various combinations of these data are shown graphically on Figures 4-3 through 4-17. Figure 4-3 shows the minimal effect a foam energy-absorbing material placed behind each bearing pad had on the overall rotor response. Figures 4-4 through 4-8 demonstrate the effectiveness of the Coulomb damping for increasing levels of unbalance, extending from the "balanced rotor" condition to 608 mg at a 1.5 in. radius (equivalent to 0.032 in.-oz. of unbalance). For additional performance comparisons, Figures 4-9 through 4-13 are also presented. These figures compare the externally unbalanced response to the "balanced rotor" response, all at the same level of external damping. Figures 4-14 through 4-17 compare the "balanced rotor" response with several levels of "unbalanced rotor" response for the undamped Hydroflex bearing.

For reference, the rotor peak-to-peak excursion can be obtained in inches from the response data as follows. For the ball bearing configuration test results, multiply the ordinate scale reading by  $1.88 \times 10^{-3}$  in.; for the fluid film bearing configuration test results, multiply by  $2.55 \times 10^{-4}$  in.

In addition to rotor response data, acquired test data also included the temperatures at the trailing edge of all four Hydroflex bearing pads (see Table 4-3). The orientation of the thermocouples relative to the gravity vector is shown in Figure 3-2 in Section 3.0.

To close out the rotor response evaluation, the Hydroflex bearing was run to 30,000 r/min with the maximum rotor unbalance at the Hydroflex end of the rotor equal to 0.032 in.-oz. No response data were taken for this run other than the pad temperatures, since the conical mode shape of the rotor excursion at high rotor speeds has the cone apex at the Hydroflex bearing. This reduces the rotor response at the test bearing to almost zero; at this condition, any damper becomes ineffective and no useful data can be acquired. The dynamics of the rotor were monitored visually, however, to determine whether any rotor instabilities became evident. None were noted in the run to 30,000 r/min.

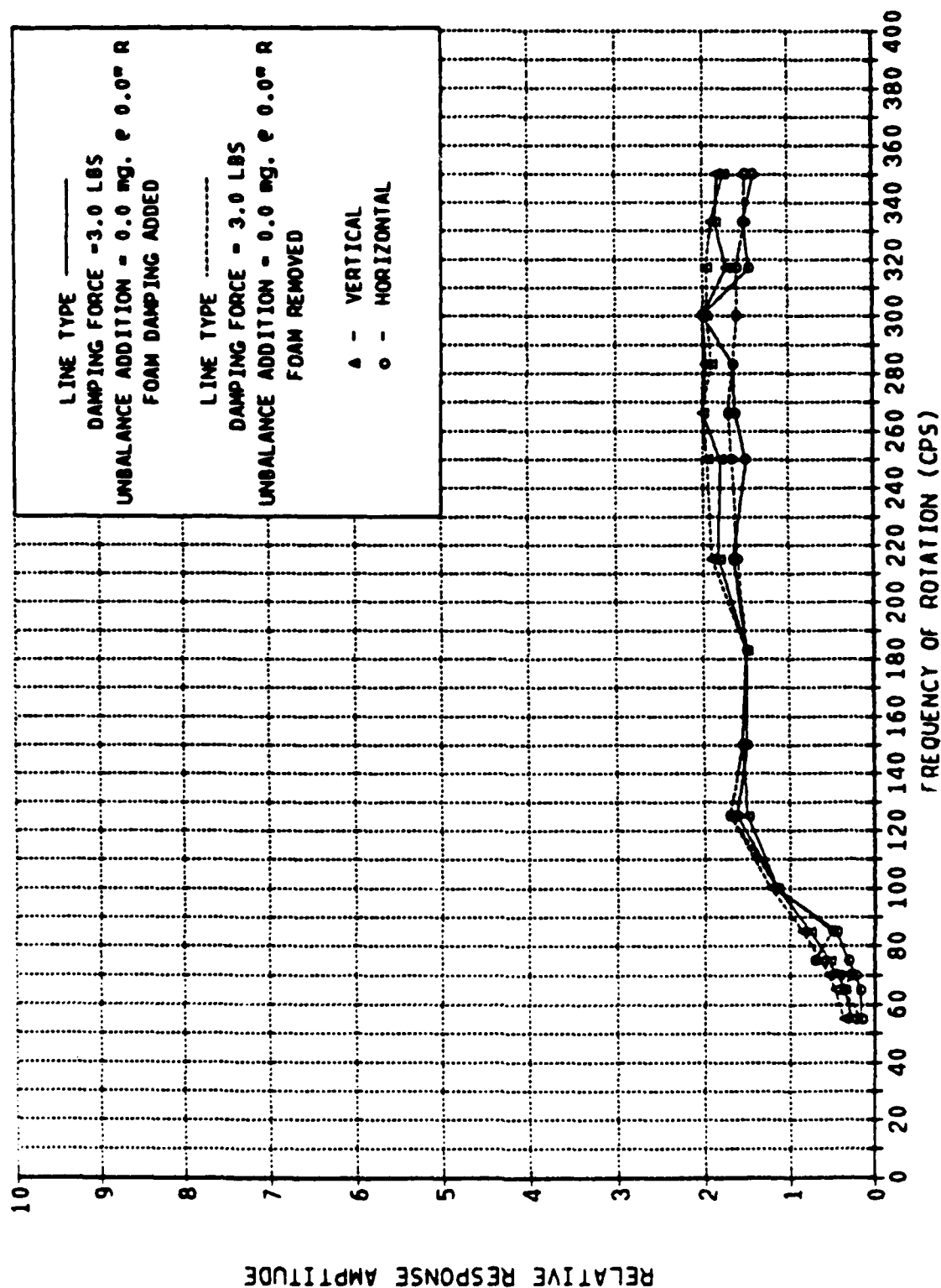


Fig. 4-3 Hydroflex<sup>TM</sup> Bearing Response; External Damping - with and without Energy Absorbing Foam Backing

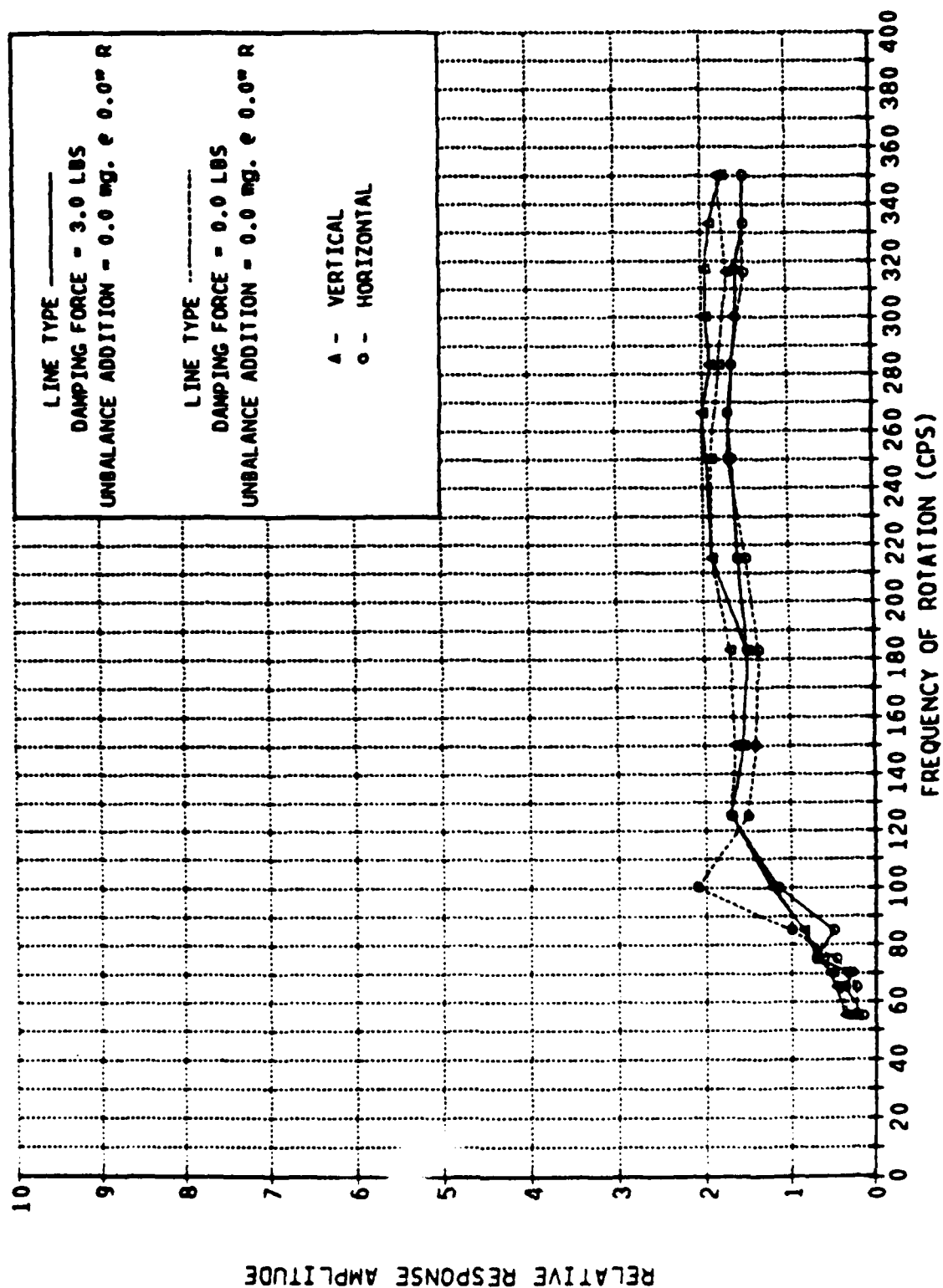


Fig. 4-4 Unbalance Response; No External Unbalance; with and without External Damping

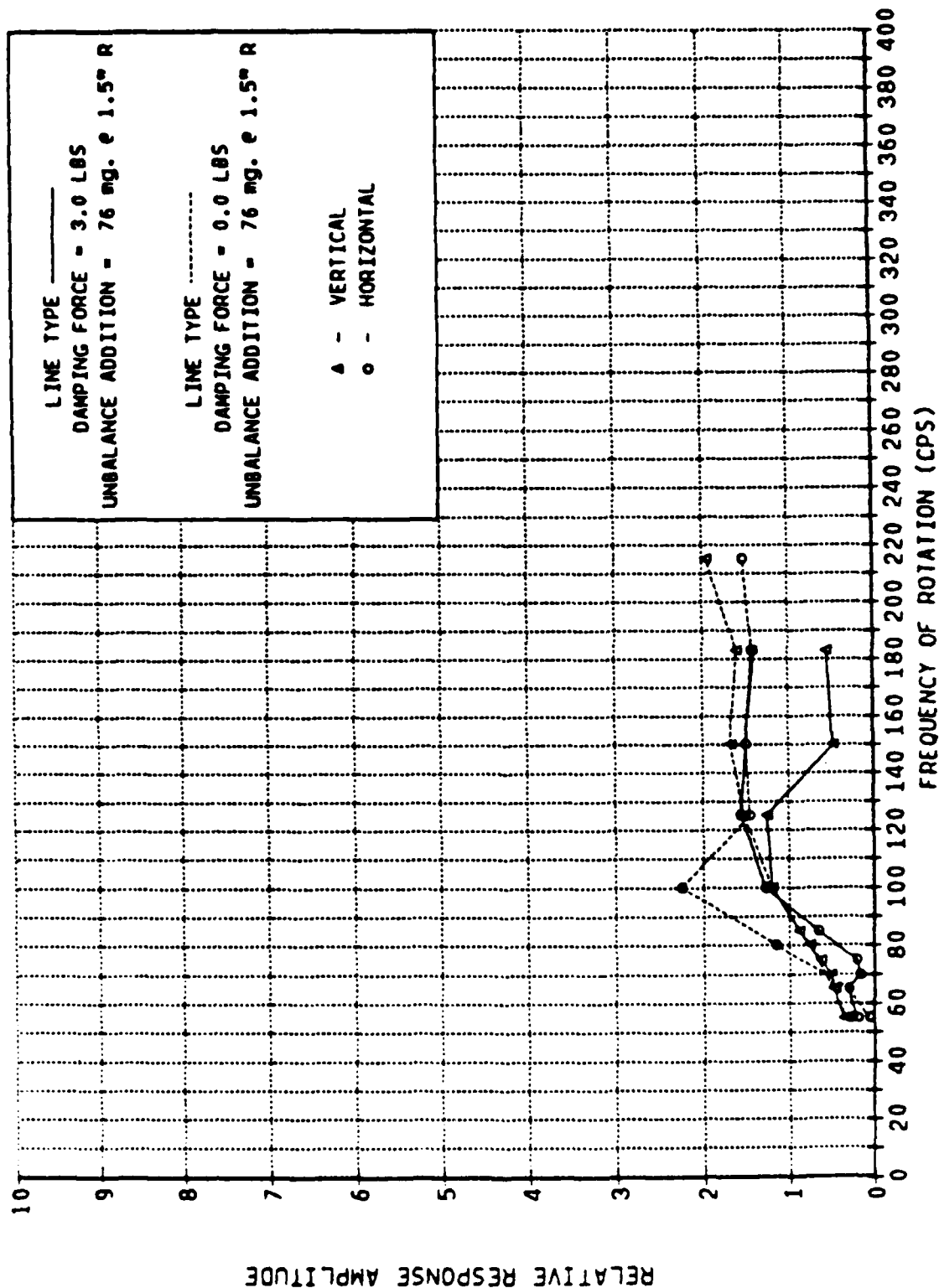


Fig. 4-5 Unbalance Response;  $4 \times 10^{-3}$  in.-oz External Unbalance; with and without External Damping

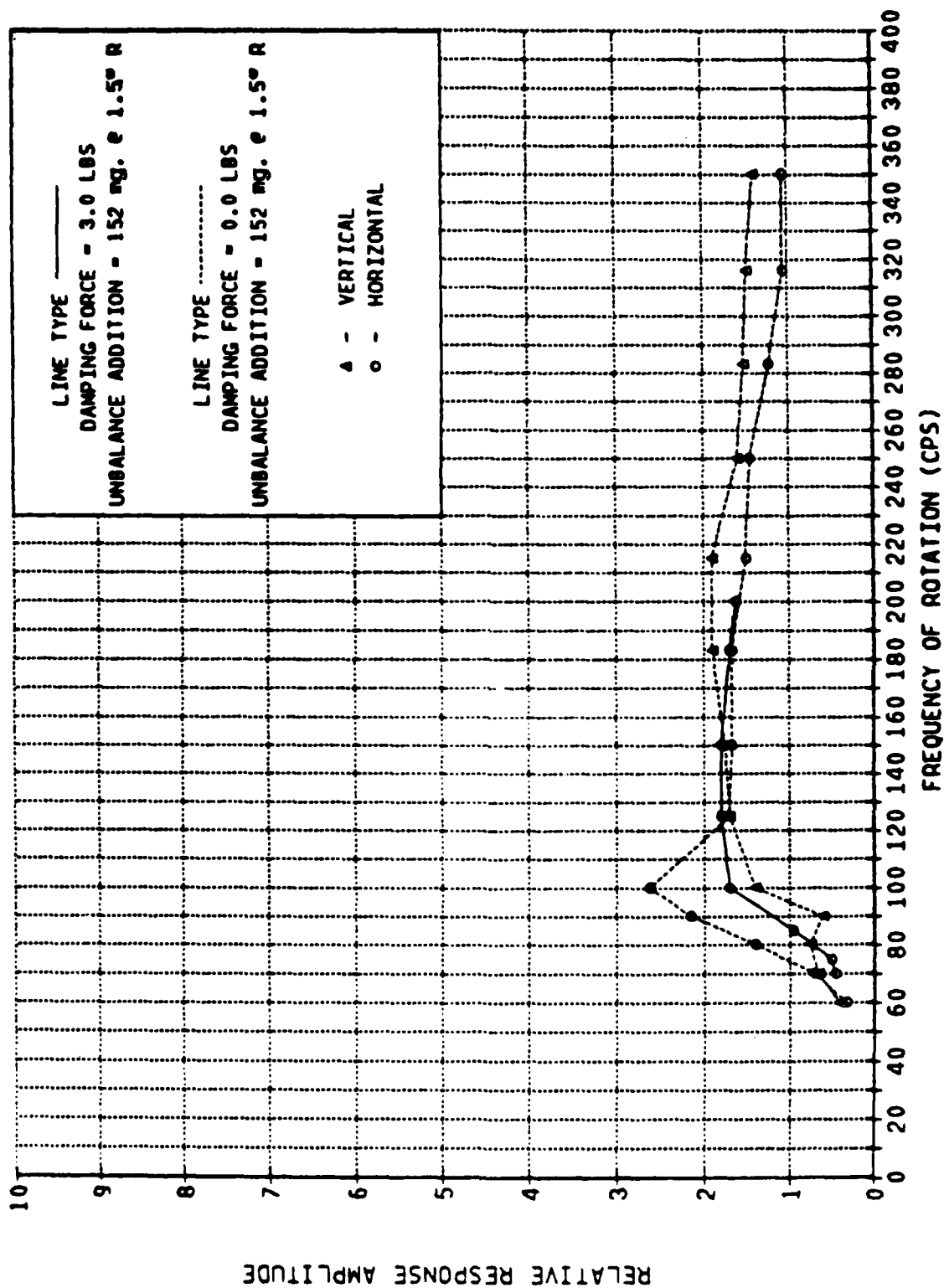


Fig. 4-6 Unbalance Response;  $8 \times 10^{-3}$  in.-oz External Unbalance; with and without External Damping

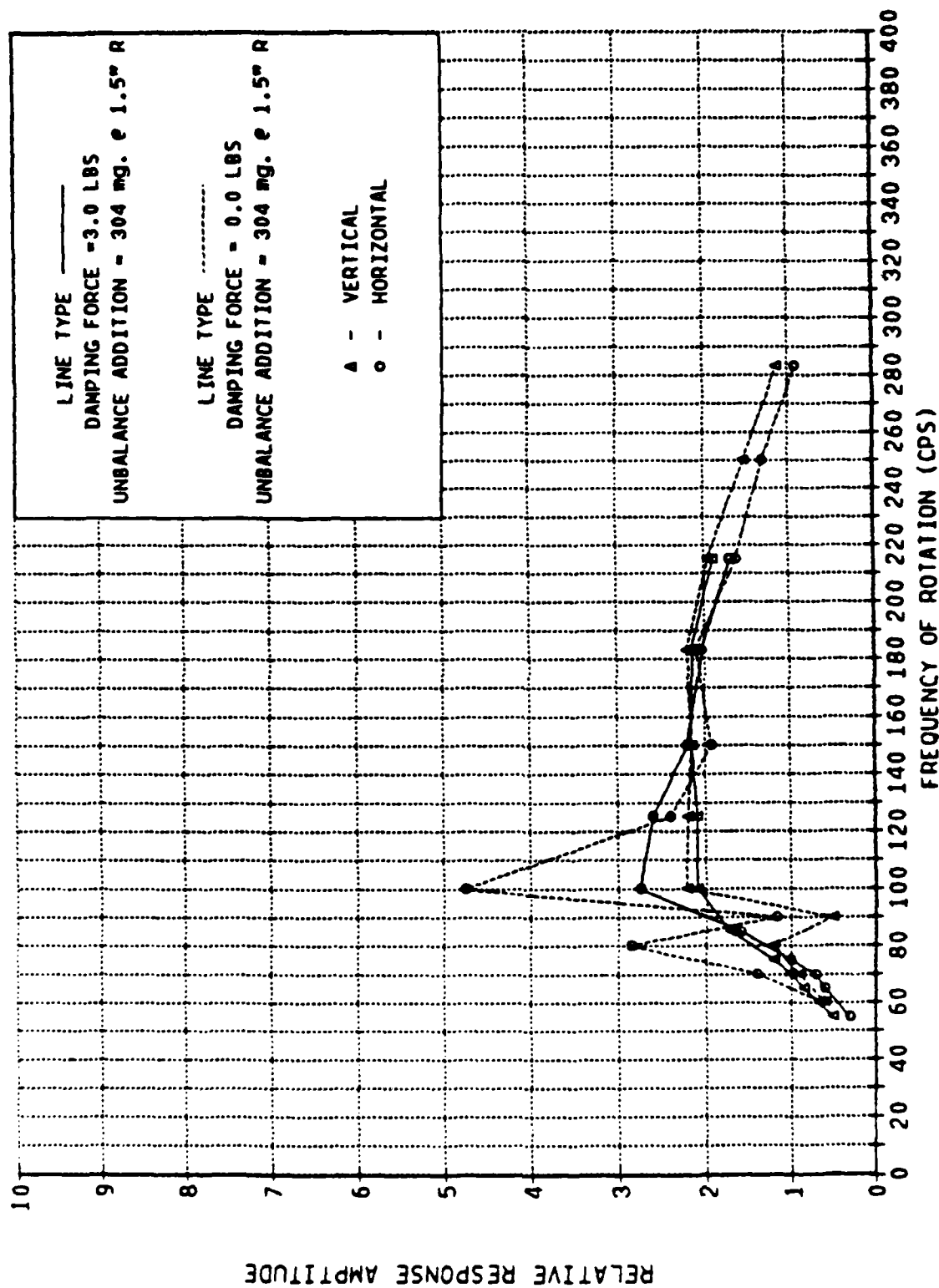


Fig. 4-7 Unbalance Response;  $16 \times 10^{-3}$  in.-oz External Unbalance; with and without External Damping

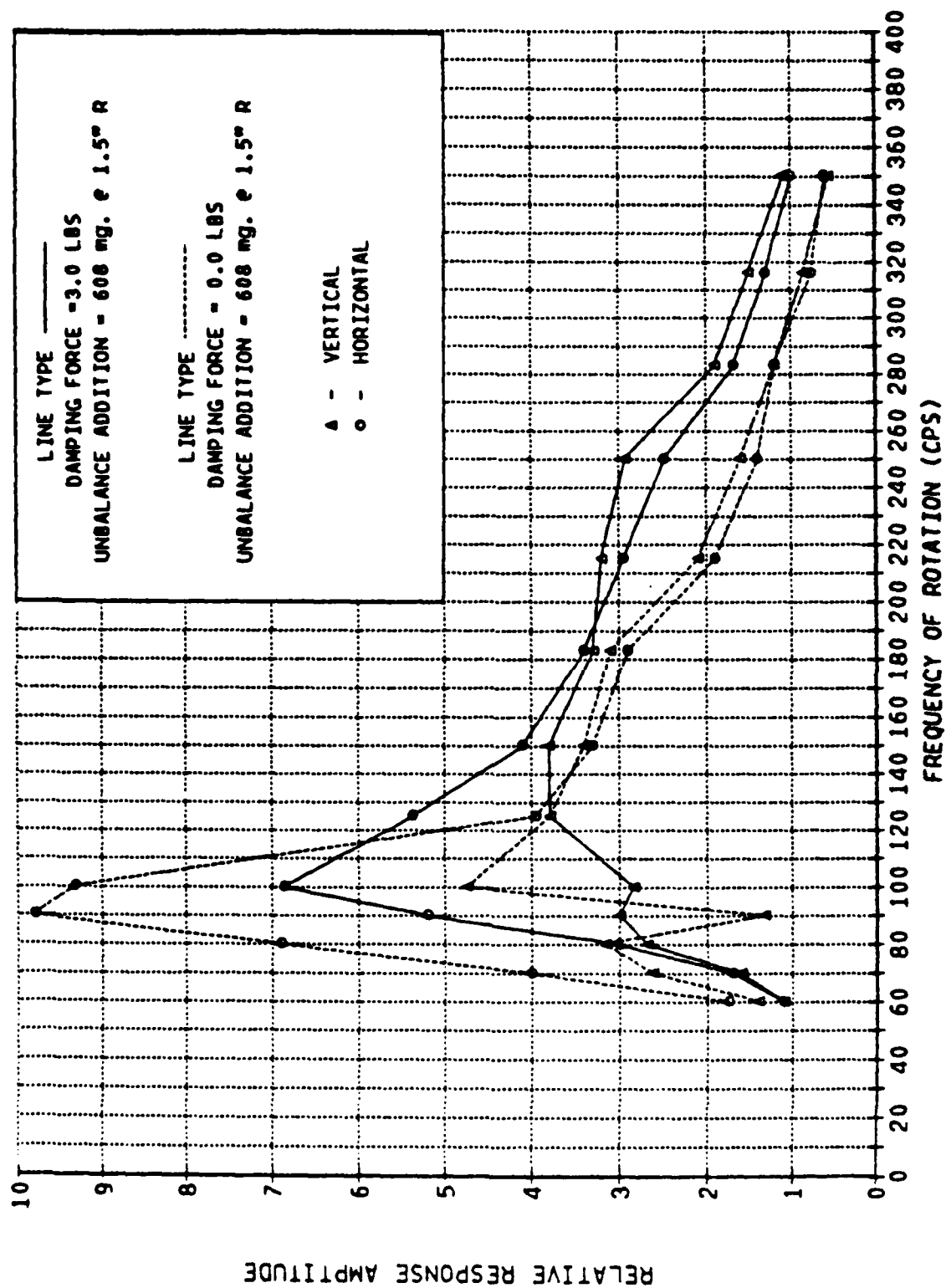


Fig. 4-8 Unbalance Response;  $32 \times 10^{-3}$  in.-oz External Unbalance, with and without External Damping



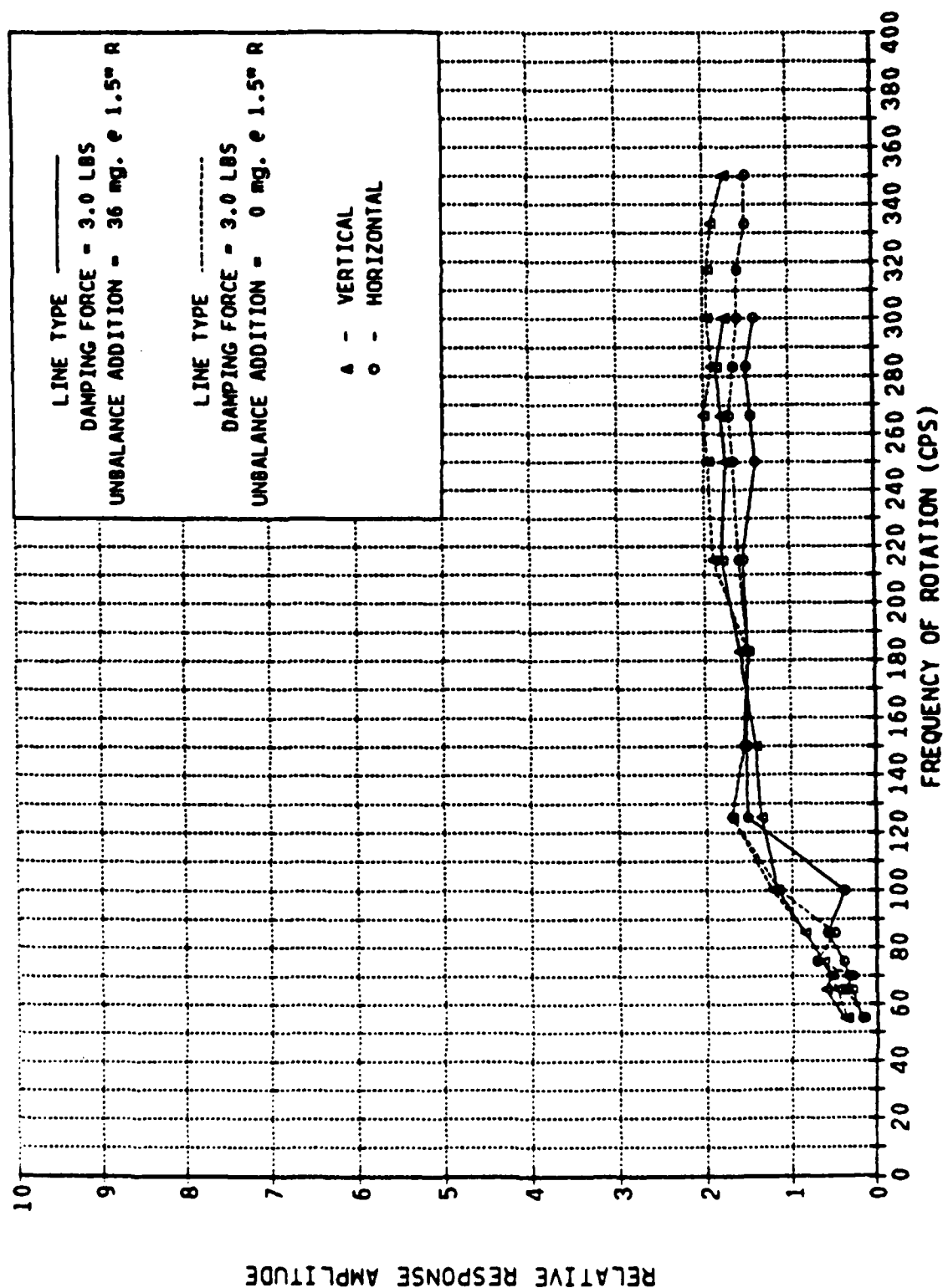


Fig. 4-9 Unbalance Response; with External Damping; with and without  $2 \times 10^{-3}$  in.-oz External Unbalance

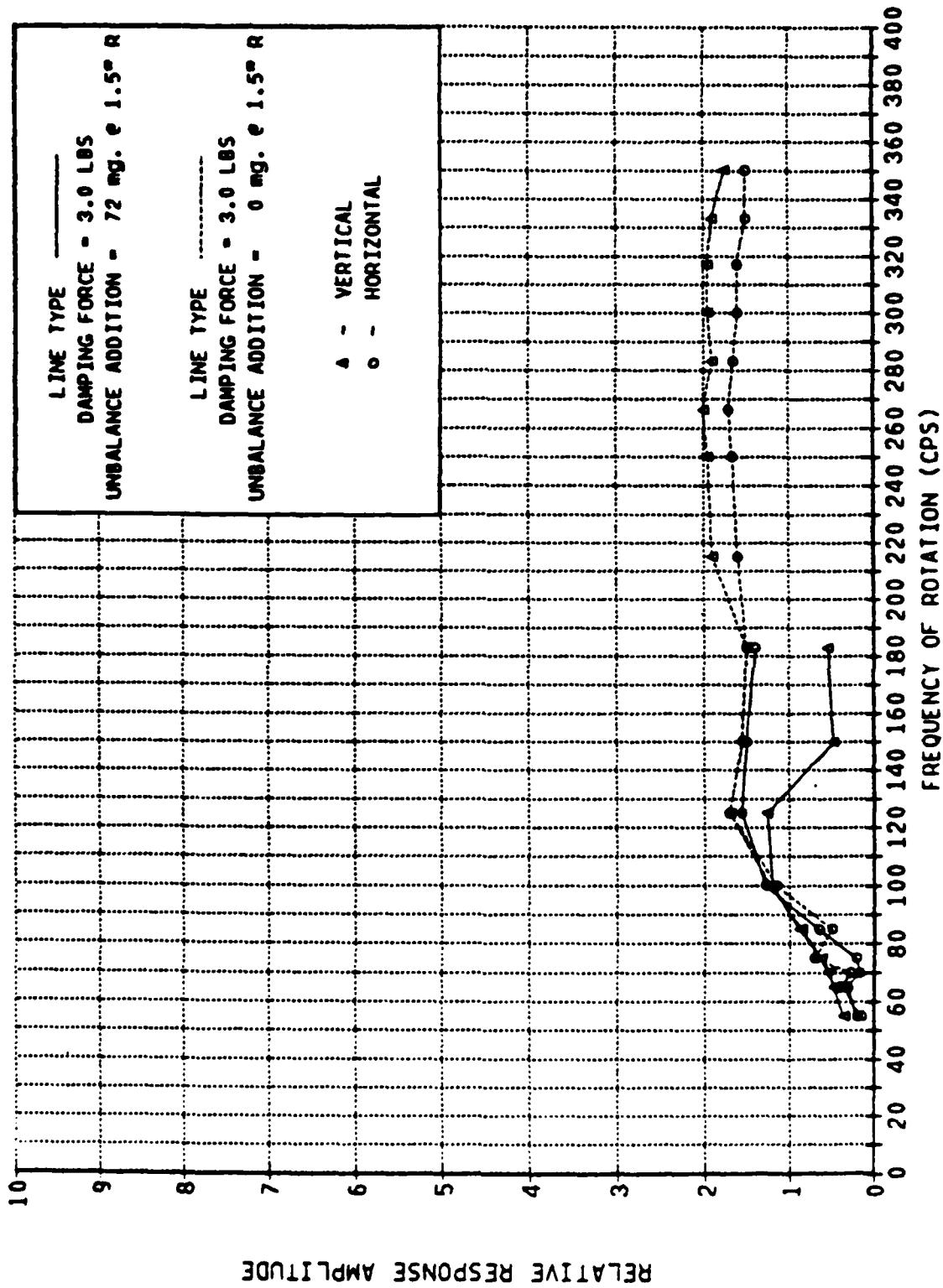


Fig. 4-10 Unbalance Response; with External Damping; with and without  $4 \times 10^{-3}$  in.-oz External Unbalance

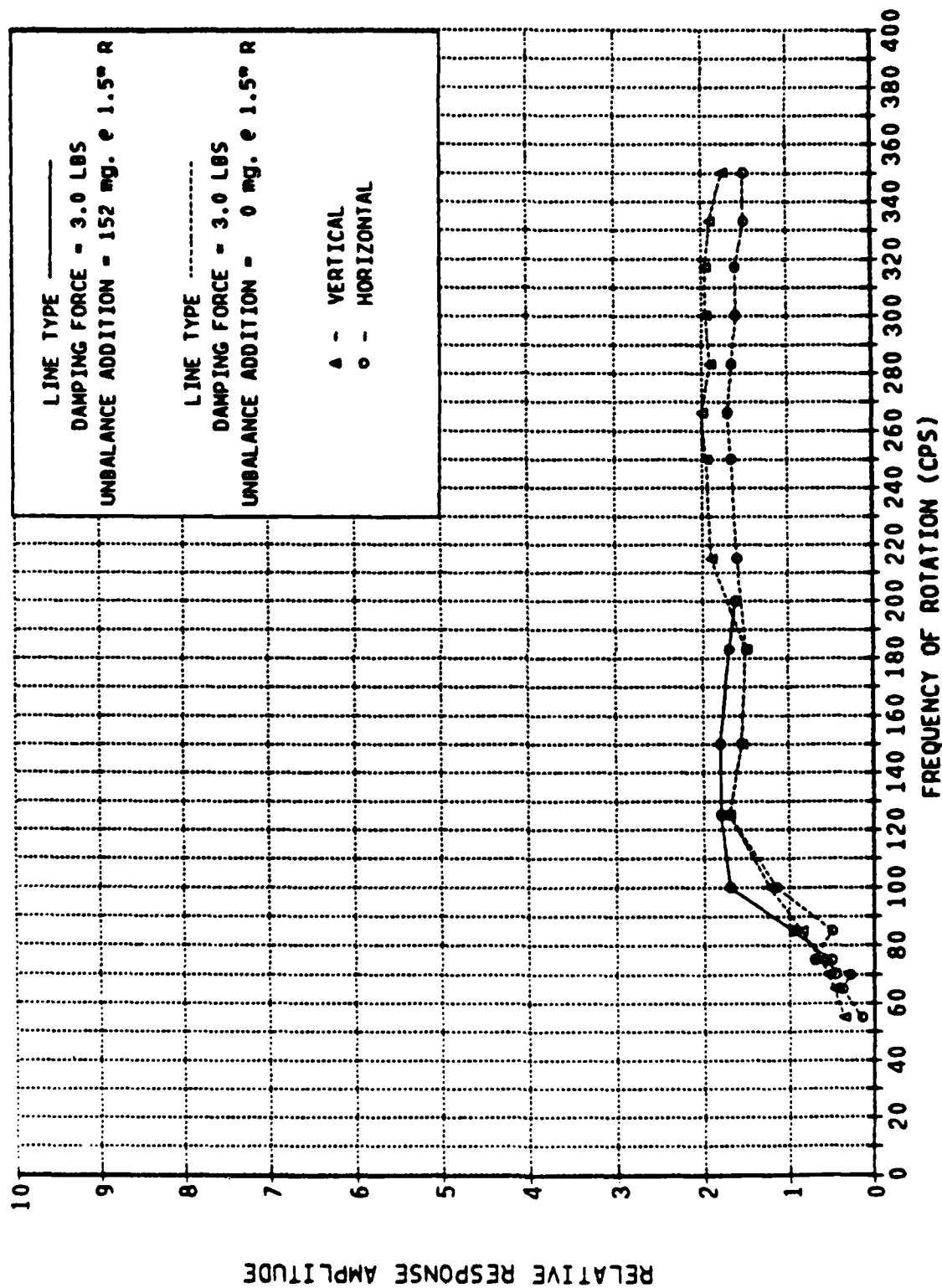


Fig. 4-11 Unbalance Response; with External Damping; with and without  $8 \times 10^{-3}$  in.-oz External Unbalance

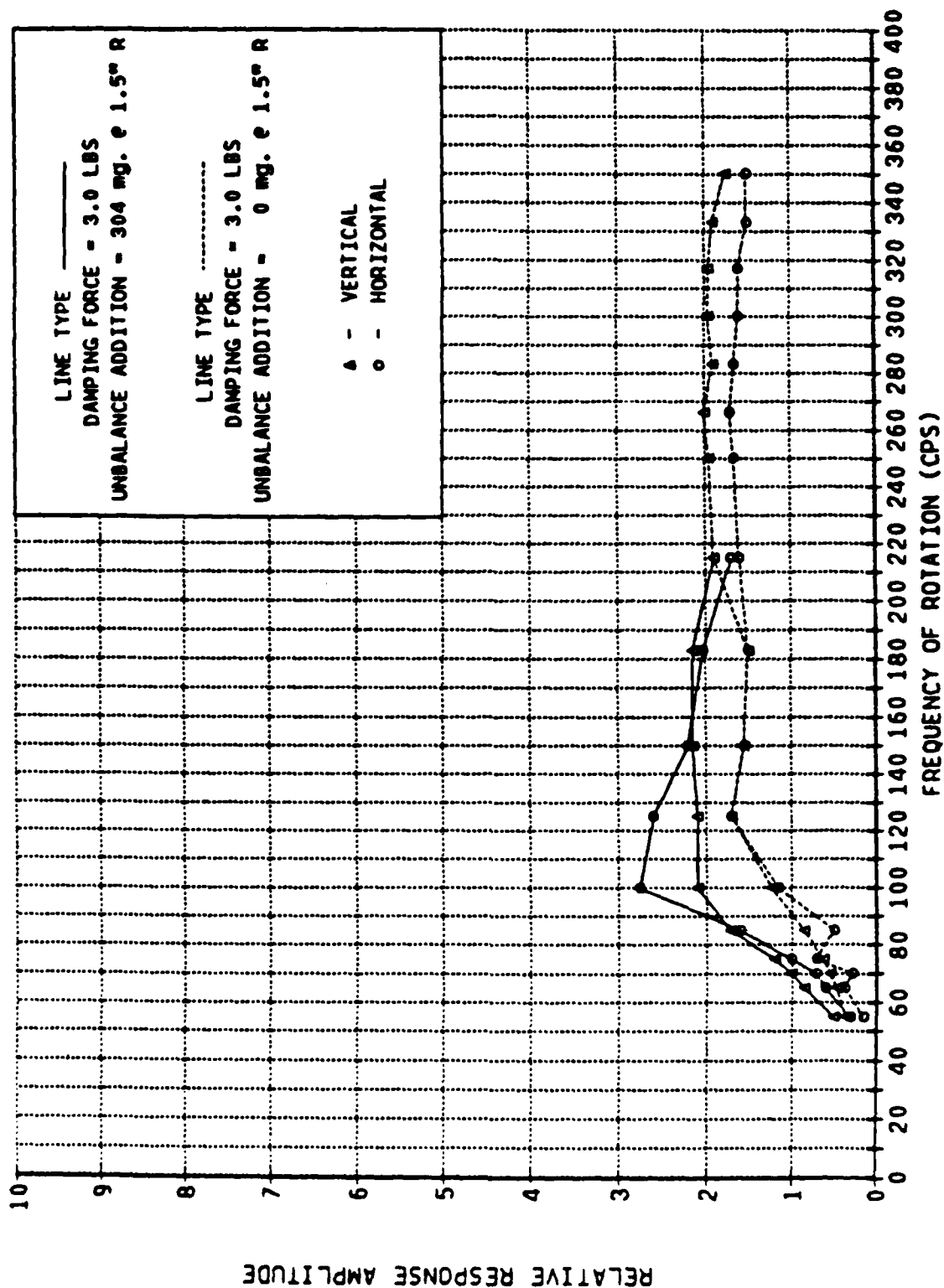


Fig. 4-12 Unbalance Response; with External Damping; with and without  $16 \times 10^{-3}$  in.-oz External Unbalance

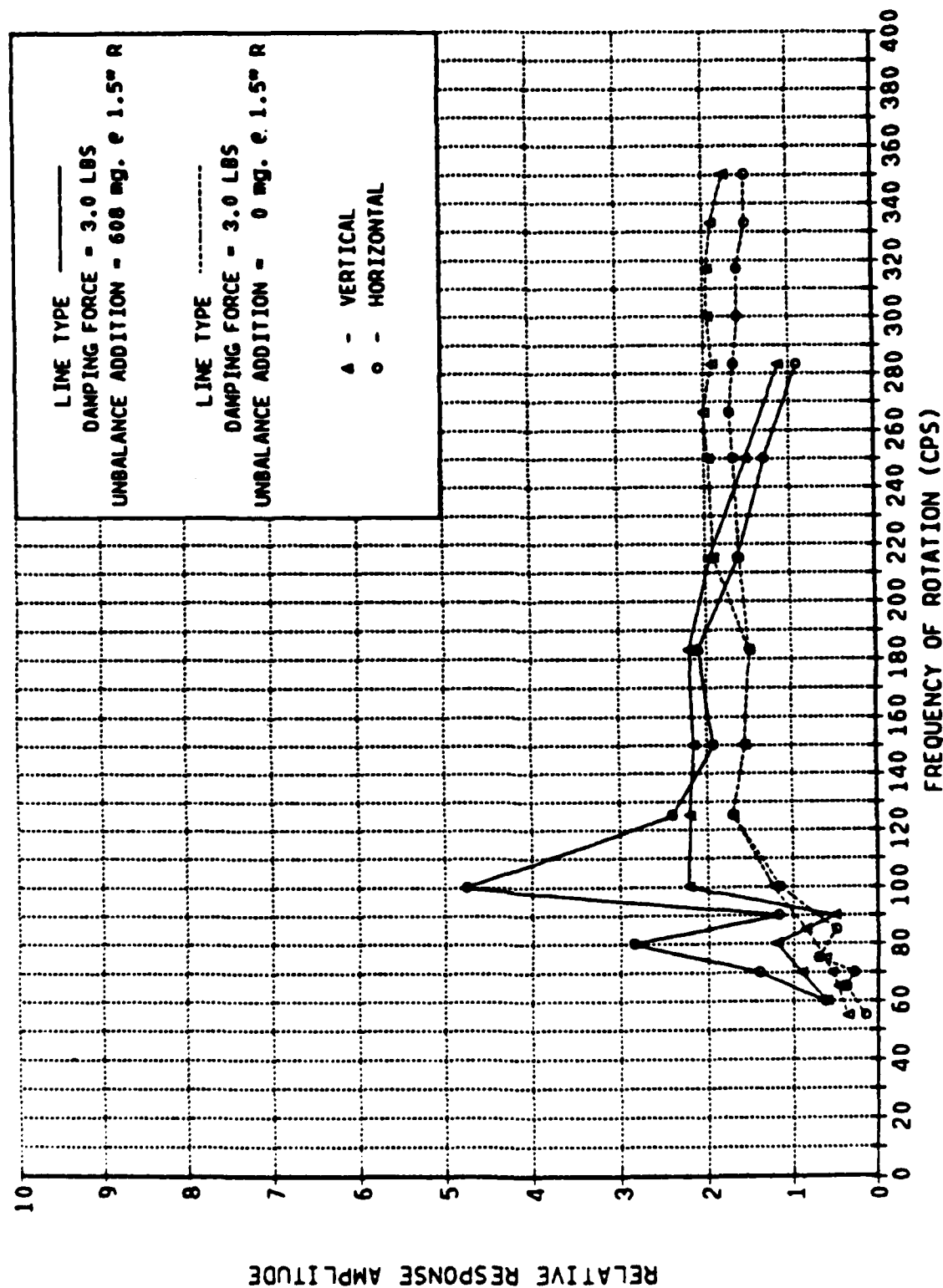


Fig. 4-13 Unbalance Response; with External Damping; with and without  $32 \times 10^{-3}$  in.-oz External Unbalance

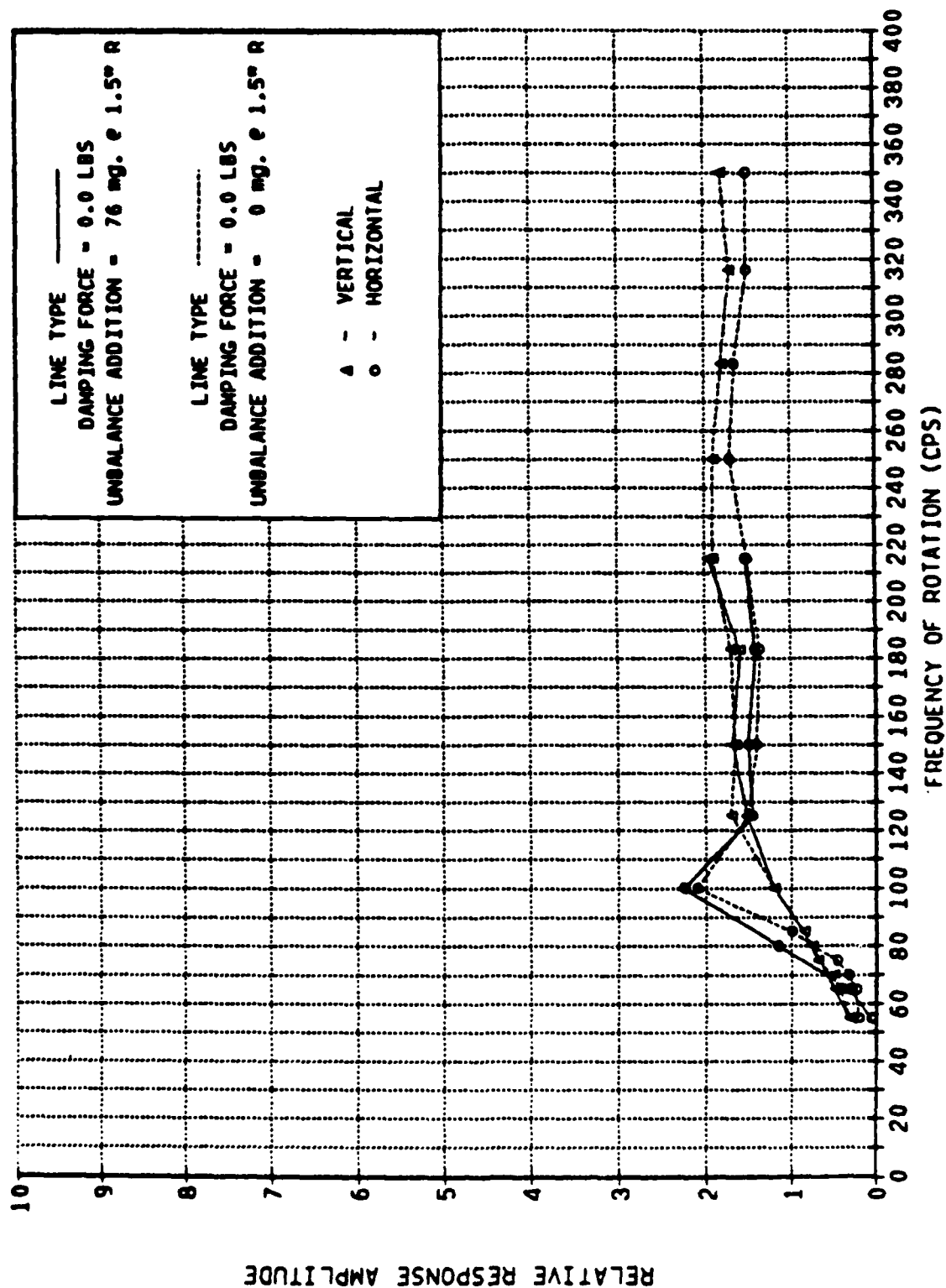


Fig. 4-14 Unbalance Response; No External Damping; with and without  $4 \times 10^{-3}$  in.-oz External Damping

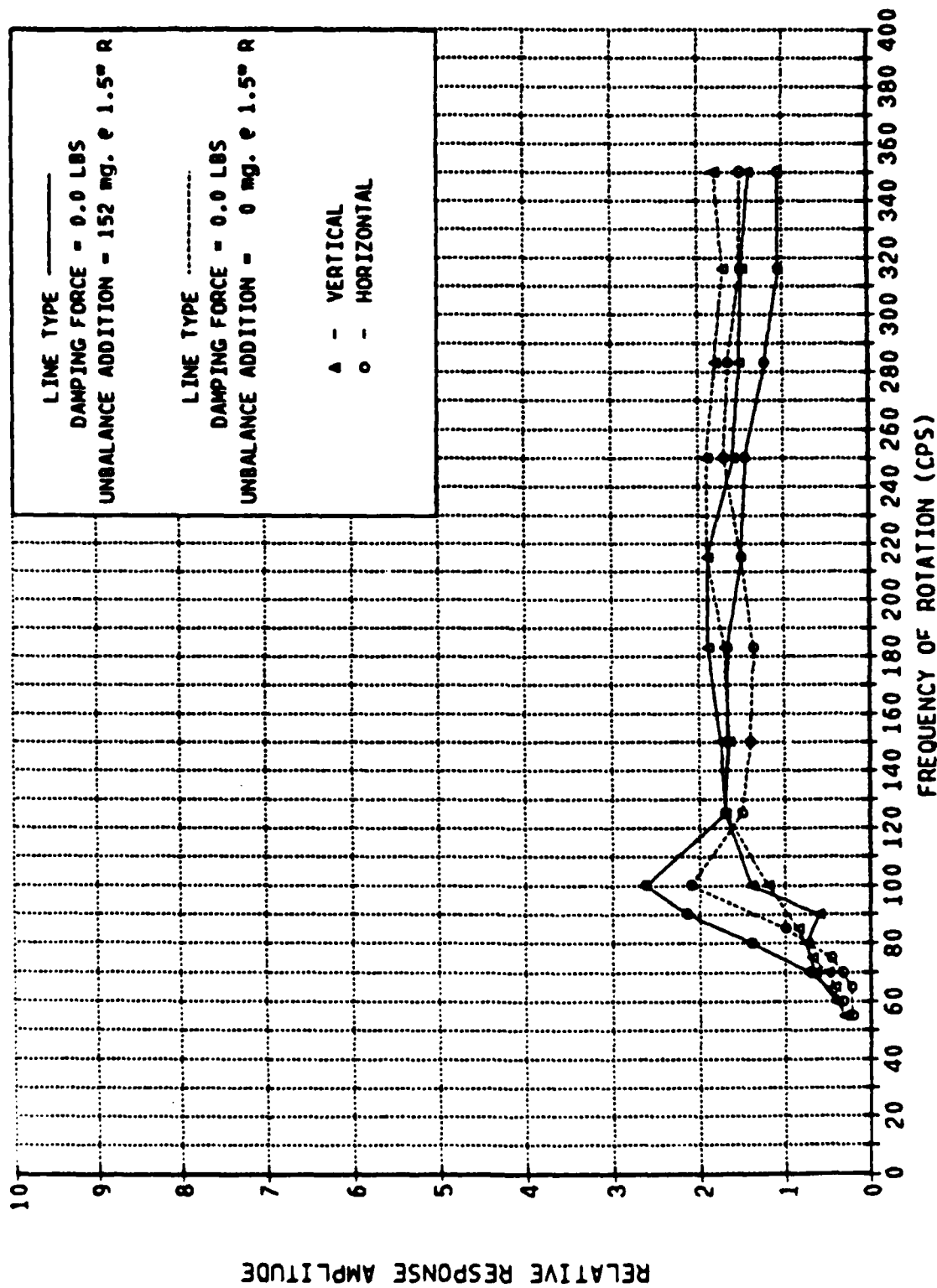


Fig. 4-15 Unbalance Response; No External Damping; with and without  $8 \times 10^{-3}$  in.-oz External Damping

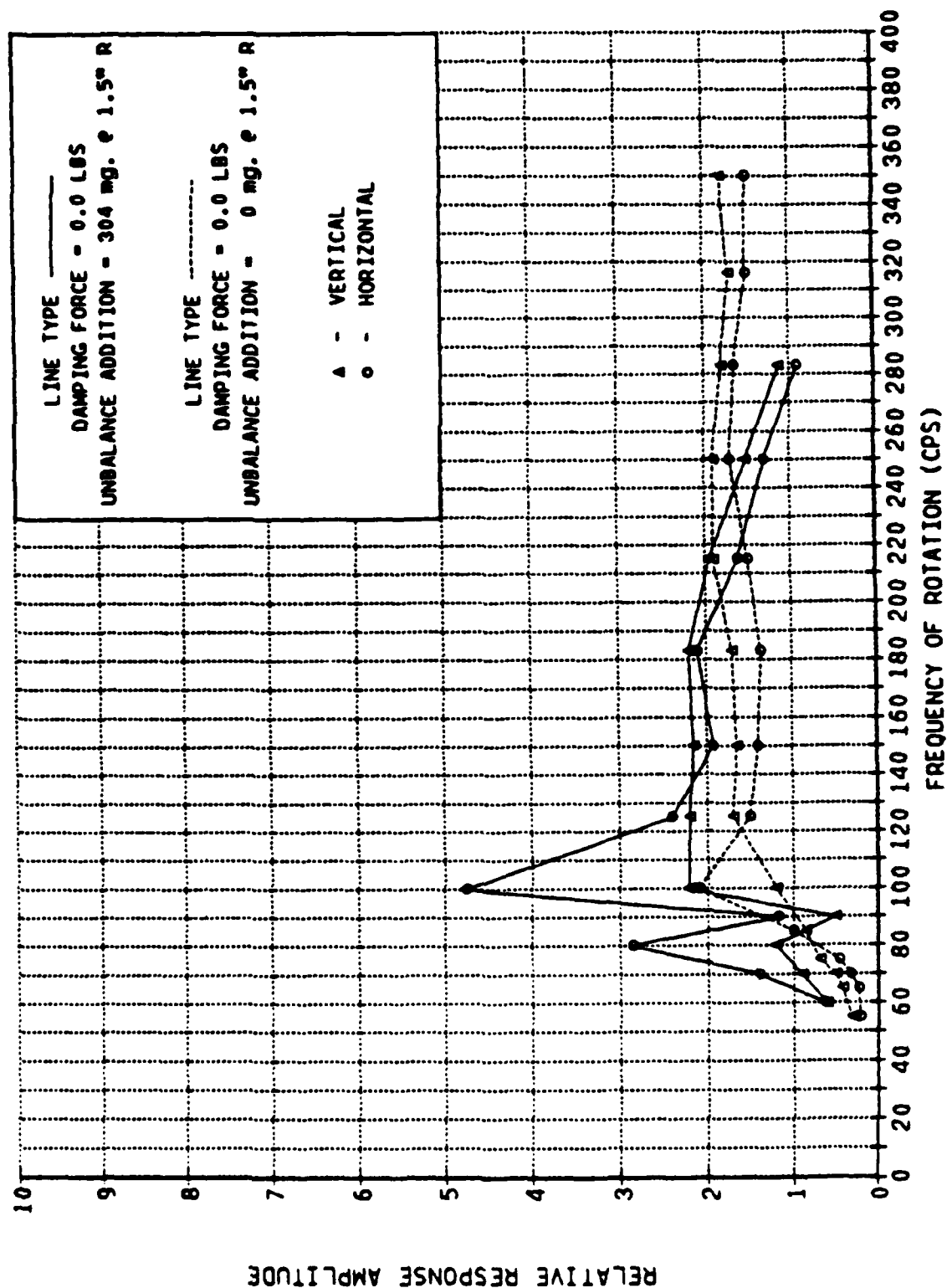


Fig. 4-16 Unbalance Response; No External Damping; with and without  $16 \times 10^{-3}$  in.-oz External Damping



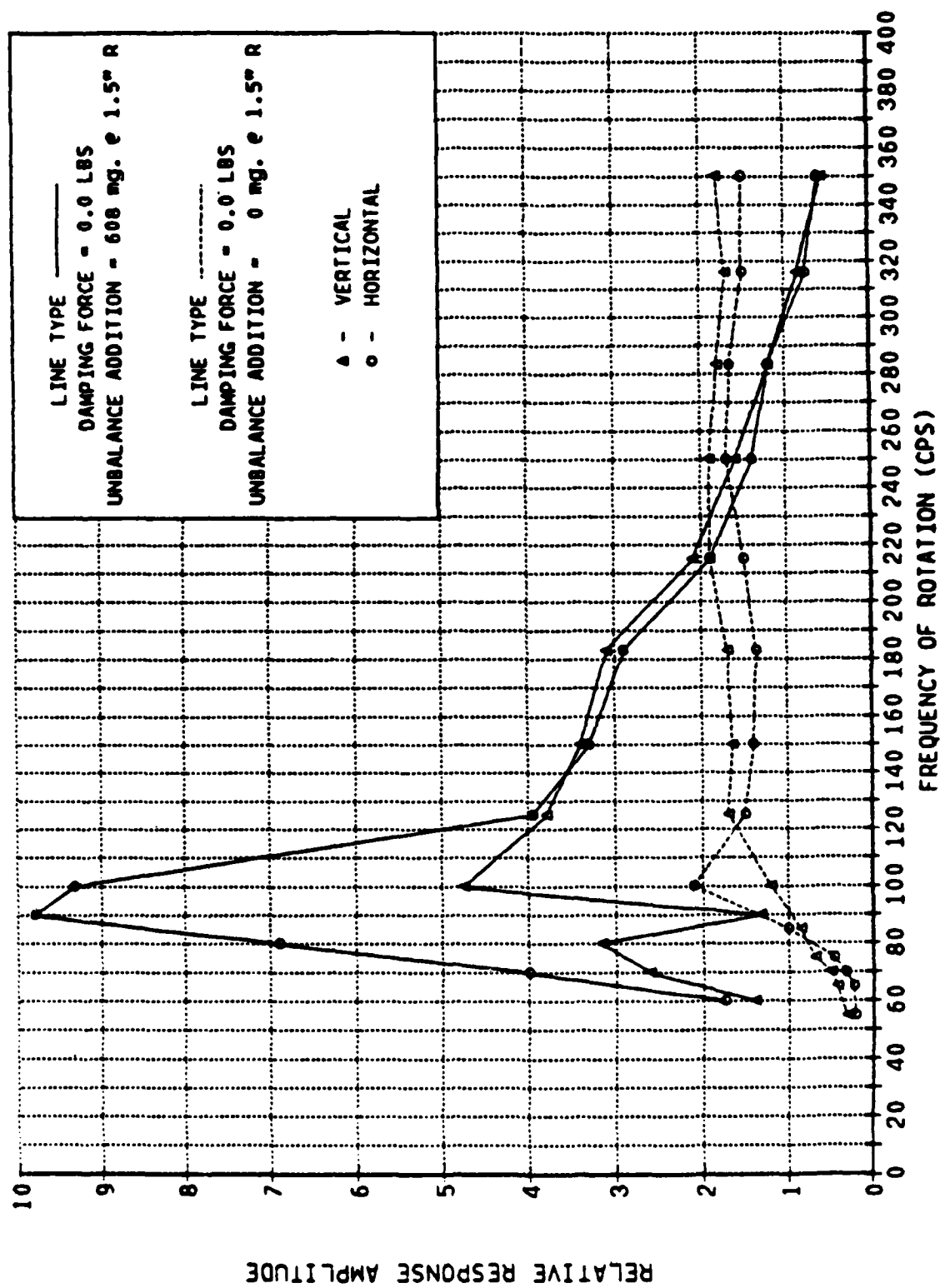


Fig. 4-17 Unbalance Response; No External Damping; with and without  $32 \times 10^{-3}$  in.-oz External Damping

TABLE 4-3

TYPICAL PAD TEMPERATURE (°F) RECORDED DURING THE TEST PROGRAM

Rotor Speed (r/min)	TC-1	TC-2	TC-3	TC-4
3,300	88	88	88	88
6,000	85	85	85	85
9,000	86	86	86	86
11,000	88	88	88	88
13,000	91	91	91	90
15,000	94	95	95	94
17,000	96	97	97	96
19,000	100	100	101	99
21,000	102	102	102	101
27,500	119	121	122	120
30,000	126	128	130	127

Ambient Temp. = 80°F

### 4.3 Effects of External Excitation

The third and last test sequence performed on the Hydroflex bearing was a study of its performance when subjected to external vibration. To perform these experiments, the complete Hydroflex test rig was suspended on four low-rate coil springs and was vibrated in the horizontal direction perpendicular to its spin axis by a small, low-force electromagnetic shaker. Figure 4-18 illustrates schematically how the test apparatus was arranged.

The method employed during this test sequence was as follows. At increments of 5,000 r/min, starting at 5,000 r/min and extending to 30,000 r/min, the shaker was energized to full power at each of four excitation frequencies spanning one-half the test speed. At each test point, the actual level of horizontal excitation was measured using a high-gain accelerometer. Both the horizontal and vertical components of the rotor motion at the Hydroflex bearing were measured for both frequency content and amplitude on a real-time frequency analyzer.

For all tests, the spring dampers were set to have a 3-lb friction force, and the rotor was unbalanced to 0.032 in.-oz at the Hydroflex bearing location.

The final results of the executed test plan are listed on Table 4-4. The most impressive result of this testing is that the Hydroflex bearing did not show any performance degradation due to the external excitation for the level of vibration input imposed. Also, the rotor response at operating speed showed little or no effect of the near one-half running speed input frequency. The excitation frequencies appeared in the rotor response, but their resulting amplitudes were small and seemed to be affected little by the changes in frequency at any given rotor speed. The only exception is found at the 10,000 and 15,000 r/min test points, which indicates a larger-than-normal amplification of the excitation frequencies in the horizontal direction. This response is not unexpected since these test speeds lie close to the calculated second critical speed of 16,960 r/min, and the excitation frequencies of one-half rotor speed would excite the nonsynchronous response.

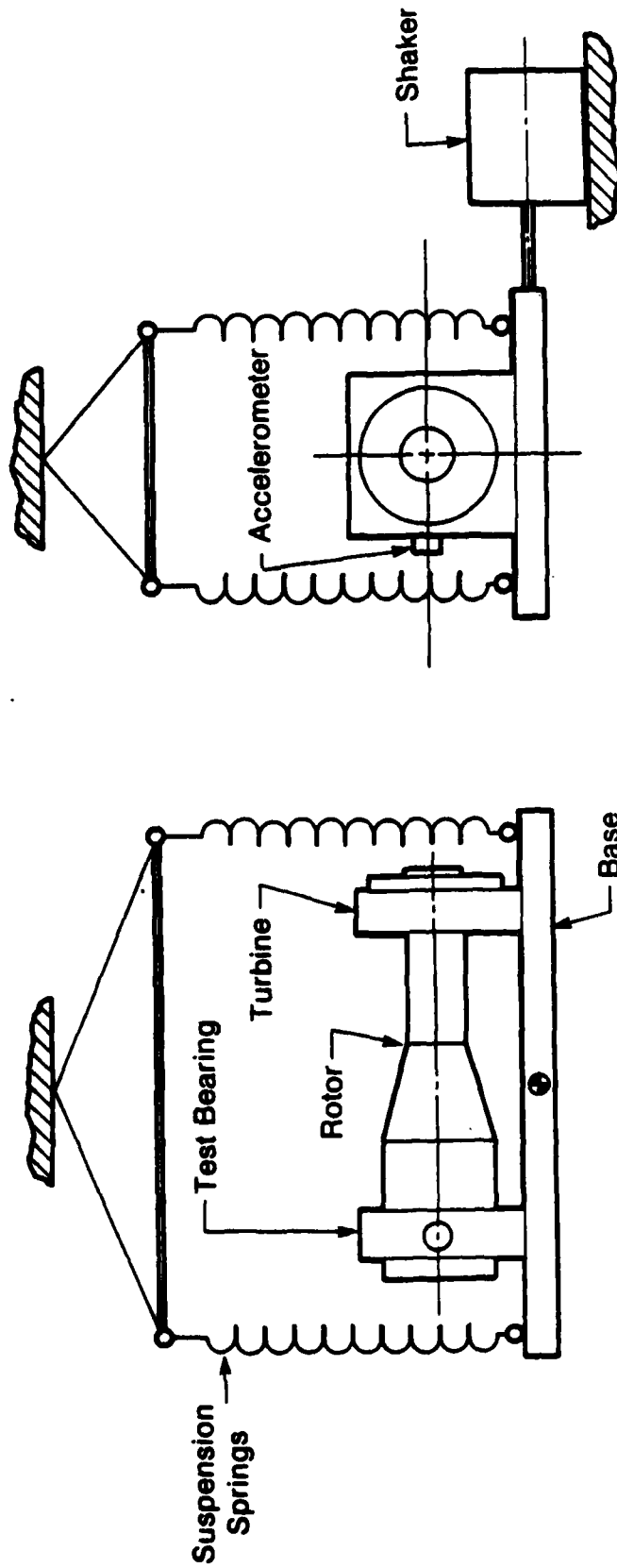


Fig. 4-18 External Excitation Test Setup

TABLE 4-4

EXTERNAL EXCITATION TEST RESULTS

Test Speed r/min (Hz)	Excitation		Bearing Axis	Rotor Response			
				At Running Freq.		At Excitation Freq.	
	Freq. (Hz)	Amp. (g)		Freq. (Hz)	Single Amp. (10 <sup>-3</sup> in.)	Freq. (Hz)	Single Amp. (10 <sup>-3</sup> in.)
5,000 (83.3)	0	0	Vert.	83.6	0.72		
	0	0	Horiz.	83.6	0.69		
			Vert.	84	0.85	40	0.03
	40	0.20	Horiz.	83.6	0.67	40	0.04
			Vert.	83.6	0.89	45	0.01
	45	0.20	Horiz.	83.6	0.67	45	0.47
			Vert.	83.2	0.87	50	0.04
	50	0.15	Horiz.	83.6	0.65	50	0.47
			Vert.	83.6	0.85	55	0.04
	55	0.10	Horiz.	84	0.65	55	0.50
10,000 (167)	0	0	Vert.	167	0.85		
	0	0	Horiz.	167	0.92		
			Vert.	167	0.88	70	0.50
	70	0.10	Horiz.	167	0.84	70	0.65
			Vert.	167	0.96	75	0.50
	75	0.10	Horiz.	167	0.87	75	0.51
			Vert.	167	0.95	80	0.52
	80	0.10	Horiz.	167	0.84	80	0.52
			Vert.	167	0.89	85	0.56
	85	0.20	Horiz.	167	0.87	85	0.56
15,000 (250)	0	0	Vert.	250	0.79		
	0	0	Horiz.	250	0.63		
			Vert.	250	0.79	114	0.32
	115	0.20	Horiz.	250	0.61	114	1.53
			Vert.	250	0.81	121	0.37
	120	0.20	Horiz.	250	0.61	121	1.16
			Vert.	250	0.80	125	0.34
	125	0.30	Horiz.	250	0.53	125	1.47
			Vert.	250	0.82	130	1.92
	130	0.30	Horiz.	250	0.62	130	0.97

TABLE 4-4 (Concluded)

Test Speed r/min (Hz)	Excitation		Bearing Axis	Rotor Response			
				At Running Freq.		At Excitation Freq.	
	Freq. (Hz)	Amp. (g)		Freq. (Hz)	Single Amp. (10 <sup>-3</sup> in.)	Freq. (Hz)	Single Amp. (10 <sup>-3</sup> in.)
20,000 (333)	0	0	Vert.	333	0.41		
	0	0	Horiz.	333	0.29		
			Vert.	334	0.39	156	0.13
	156	0.20	Horiz.	334	0.29	156	0.50
			Vert.	333	0.39	161	0.20
	161	0.10	Horiz.	334	0.30	161	0.40
			Vert.	334	0.40	166	0.18
	166	0.20	Horiz.	334	0.30	166	0.33
			Vert.	334	0.39	170	0.23
	170	0.20	Horiz.	333	0.31	170	0.24
25,000 (415)	0	0	Vert.	416	0.24		
	0	0	Horiz.	416	0.13		
			Vert.	415	0.25	200	0.29
	200	0.10	Horiz.	416	0.14	200	0.21
			Vert.	416	0.28	205	0.13
	205	0.10	Horiz.	416	0.12	204	0.20
			Vert.	416	0.26	210	0.24
	210	0.40	Horiz.	416	0.11	210	0.15
			Vert.	416	0.27	216	0.10
	215	0.30	Horiz.	416	0.13	216	0.14
30,000 (500)	0	0	Vert.	500	0.24		
	0	0	Horiz.	500	0.24		
			Vert.	500	0.27	240	0.04
	240	>0.1	Horiz.	500	0.24	240	0.08
			Vert.	500	0.27	244	0.02
	245	>0.1	Horiz.	500	0.23	244	0.08
			Vert.	500	0.25	250	0.06
	250	>0.1	Horiz.	500	0.22	250	0.06
			Vert.	500	0.25	256	0.03
	255	>0.1	Horiz.	500	0.21	256	0.06

## 5.0 DISCUSSION OF TEST RESULTS

The most significant results of the Hydroflex™ bearing evaluation were the dynamic tests confirming the feasibility of the Hydroflex bearing concept. These tests, performed to provide a dynamic evaluation of damping rates, include data points 3, 4, 5, 6 and 7 of Table 4-2 at zero damper force and data points 9, 10, 11, 12 and 13 at a 3-lb. damper force. The graphical comparison of these runs is shown in Figures 4-4 through 4-17. Experimental verification of the analytical estimate for Hydroflex bearing flexure stiffness was also achieved as shown by the data included in Table 4-1. The radial static flexure stiffness determined experimentally is well within the expected deviation from that obtained analytically.

The response of the Hydroflex bearing to various levels of unbalance is shown by all dynamic tests (data points 3 through 13). From these tests, various combinations of data were plotted for comparison. Figures 4-4 through 4-8 compare undamped to damped response at the same level of unbalance. Figures 4-9 through 4-13 compare various unbalance levels with no unbalance, all at the same fixed external damper setting. Figures 4-14 through 4-17 provide the same comparisons without external damping. In all cases, a change in unbalance resulted in an approximately linear change in peak response, indicating a nearly linear system.

For the Hydroflex bearing tests reported herein, the response of the test rotor near the lower critical speed produced an elliptical orbit. When the rotor traversed this critical speed and the phase angle between the forcing function (unbalance) and rotor motion (response) changed, the orientation of the response ellipse major axis rotated from a positive through zero to a negative slope. As this rotation occurred, the response amplitude, in both the vertical and horizontal directions, first increased, then decreased through a minimum value before increasing to a maximum response level. This produced the double peak response curves seen on the majority of the experimental response curves.

Each of the experimental response curves was examined to determine what the radial damping coefficient might be. It was not until the high unbalance of

0.016 in.-oz (304 mg at R = 1.5 in.) or greater was tested, however, that sufficient response amplitude was attained to actually measure damping effects.

At unbalance levels below 0.016 in.-oz, the rotor response at the externally damped Hydroflex bearing appears as a critically damped response with no sharply defined peak. Even though the effect of damping is visually evident, as seen by the reduction in amplitude at the 100 cycles per second critical speed, it is only at unbalance levels of 0.016 and above that there is sufficient definition of a sharp response peak to permit damping coefficient calculations.

In calculating the level of system damping, the sharpness or width of the response curve at resonance is used. A good approximation of damping values is obtained by designating the width of the response curve,  $\Delta\omega$ , at the half power point (the response amplitude equal to the maximum response divided by  $\sqrt{2}$ ) and setting the ratio of  $\Delta\omega/\omega_n$  ( $\omega_n$  = frequency at the maximum response) equal to  $1/Q$ . The actual equivalent damping coefficient is then obtained from the relationship

$$1/2Q = B/B_c = B/2M\omega_n$$

where M is the rotor mass acting on the test bearing and B the damping coefficient.

Table 5-1 lists the results of damping calculations for the 0.016 and 0.032 in.-oz unbalance tests.

Two properties of Hydroflex damping are evident from the test results. One is that the level of inherent internal damping of the bearing increases with increasing levels of unbalance. This effect is most likely caused by a greater approach velocity and larger squeeze film forces that result from the greater response amplitude at any fixed speed when operating with higher unbalance levels.



TABLE 5-1

EXPERIMENTAL DAMPING COEFFICIENTS FOR THE HYDROFLEX™ BEARING

Unbalance (in.-oz)	External Damping (lb)	Angular Velocity $\omega$ (rad/s)	$\Delta\omega$	$\Delta\omega/\omega$	Resonance Q Factor	Damping Ratio r (in.)	Damping Coefficient B (lb/s/in.)
0.016	0	100	19	0.19	5.26	0.095	5.44
0.016	3	100	96	0.96	1.04	0.49	28.1
0.032	0	95	23	0.24	4.2	0.12	6.88
0.032	3	100	100	0.42	2.4	0.21	12.0

The second property seen in the test results is the decrease in overall damping with increases in unbalance. This is consistent with the low unbalance test data, which carries the implication of a critically or overdamped system. This effect may be explained by the fact that the external Coulomb dampers used in these tests provide a fixed level of damping independent of velocity, and as unbalance levels are increased, the energy required to suppress the response is also increased without the accompanying increase in available damping energy.

The last test sequence performed on the Hydroflex bearing was an evaluation of the bearing's capability to tolerate low levels of external vibration at the most likely frequency to produce fractional frequency whirl. The external excitation was imposed at a nominal 0.2-g level in the frequency ratio range of  $0.42 N \leq f \leq 0.52 N$ . Holding the excitation g levels constant and increasing the excitation frequencies, the excitation amplitude naturally decreased. This is also demonstrated by the nonsynchronous rotor response which shows the same trend. The only deviation from this trend is at the running speeds of 10,000 and 15,000 r/min which show larger amplifications of the excitation frequency than would otherwise be expected. This may be explained by the proximity of the actual second critical speed to the running speed and the increased susceptibility of the Hydroflex bearing at this frequency to the nonsynchronous excitation.

## 6.0 CONCLUSIONS AND RECOMMENDATIONS

The initial demonstration testing of the Hydroflex™ bearing met with considerable success. The desired top speed of 30,000 r/min was reached, along with sufficient unbalance response data to confirm the successful application of Coulomb damping for reducing response amplitudes while traversing a critical speed. The demonstrated resistance of the Hydroflex bearing to external vibration also demonstrates the viability of this bearing type. The ability to operate for long periods of time with substantial flexing of the Hydroflex flexures adds to the confidence of long-term, safe operation of this bearing type.

The success of these preliminary tests provides the impetus for initiating further development work on the Hydroflex concept so that a satisfactory, equipment-rated Hydroflex bearing can become an operational reality. Some of the questions that must be answered about the Hydroflex bearing prior to its acceptance as a viable system addition (not necessarily in the order presented) are:

- What are its maximum load capacity and its operating radial stiffness, and how does it behave when designated as the sole radial rotor support in a turbomachine simulator?
- What are its thermal capabilities when designed for high-temperature operation, and how well does it actually accommodate thermal and centrifugal growth?
- Are there alternative means of providing damping, such as air dampers, which may be less susceptible to wear?
- How does extension of the Hydroflex bearing to substantially larger diameters affect its design and performance?
- What design considerations must be met, and how will the Hydroflex bearing concept perform when configured to act as an intershaft damper on advanced turbine engine designs?

- How well will a Hydroflex thrust bearing perform?

Satisfactory answers to these questions will allow a new and useful bearing to be added to the rotating machinery designer's storehouse of specialized-application bearings.

END

10-86

DTIC